

Universidade Estadual de Campinas

Pedro Carvalhaes Dias

Um Novo Sensor de Umidade de Solo de Pulso de Calor de Alta Sensibilidade, Baseado em um Único Transistor Bipolar de Junção *npn*

A Novel High Sensitivity Single Probe Heat Pulse Soil Moisture Sensor Based on a Single *npn* Bipolar Junction Transistor

Dissertação de Mestrado apresentada à Faculdade de Engenharia Elétrica e de Computação como parte dos requisitos para obtenção do título de Mestre em Engenharia Elétrica. Área de concentração: Eletrônica, Microeletrônica e Optoeletrônica.

Dissertation submitted to the School of Electrical and Computer Engineering in partial fulfillment of the requirements for the degree of Master in Electrical Engineering. Area: Electronics, Microelectronics and Optoelectronics.

Orientador: Prof. Dr. Elnatan Chagas Ferreira

Adviser: Prof. Dr. Elnatan Chagas Ferreira

Campinas, SP
2012

FICHA CATALOGRÁFICA ELABORADA PELA
BIBLIOTECA DA ÁREA DE ENGENHARIA - BAE - UNICAMP

D543n Dias, Pedro Carvalhaes

A novel high sensitivity single probe heat pulse soil moisture sensor
Based on a Single npn Bipolar Junction Transistor.
/ Pedro Carvalhaes Dias. – Campinas, SP: [s.n.], 2012.

Orientador: Elnatan Chagas Ferreira.
Dissertação (mestrado) - Universidade Estadual de Campinas,
Faculdade de Engenharia Elétrica e de Computação.

1. Detectors. 2. Soil - Moisture 3. Precision Agriculture.
4. Agriculture and technology. 5. Bipolar transistors.
I. Ferreira, Elnatan Chagas. II. Universidade
Estadual de Campinas. Faculdade de Engenharia Elétrica
e de Computação. III. Título

Título em Português: Um novo sensor de umidade de solo de pulso de calor
de alta sensibilidade, baseado em um único transistor
bipolar de junção npn

Palavras Chave em Português: Detectores, Solos - Umidade, Agricultura de
precisão, Agricultura e tecnologia, Transistores bipolares

Área de concentração: Eletrônica, Microeletrônica e Optoeletrônica.

Titulação: Mestre em Engenharia Elétrica

Banca Examinadora: Vicente Idalberto Becerra Sablón, Wilmar Bueno de Moraes

Data da defesa: 22/03/2012

Programa de Pós-Graduação: Engenharia Elétrica

COMISSÃO JULGADORA - TESE DE MESTRADO

Candidato: Pedro Carvalhaes Dias

Data da Defesa: 22 de março de 2012

Título da Tese: "A Novel High Sensitivity Single Probe Heat Pulse Soil Moisture Sensor Based on a Single npn Bipolar Junction Transistor"

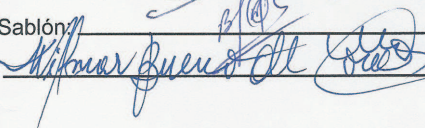
Prof. Dr. Elnatan Chagas Ferreira (Presidente):



Prof. Dr. Vicente Idalberto Becerra Sablón:



Prof. Dr. Wilmar Bueno de Moraes:



Resumo

A constante preocupação em aumentar a produtividade das plantações de uma forma sustentável e otimizando o uso dos insumos agrícolas (água, fertilizantes, pesticidas e produtos para correção do PH) levou ao desenvolvimento da agricultura de precisão, que permite determinar a quantidade correta de insumos para cada região do solo (tipicamente um hectare), evitando o desperdício.

Sensores de umidade de solo de baixo custo e fácil aplicação no campo são fundamentais para permitir um controle preciso da atividade de irrigação, sendo que os sensores que melhor atendem estes requisitos são os chamados sensores de dissipação de calor ou sensores de transferência de calor.

Estes sensores, entretanto, apresentam um problema de baixa sensibilidade na faixa de umidade mais importante para as plantas (umidade de solo θ_v variando entre 5% e 35%), pois, para cobrir esta variação de 30% em θ_v com resolução de 1%, é necessário medir variações de temperatura de aproximadamente 0,026 °C nos sensores de pulso de calor a duas pontas e 0,05 °C para os sensores de pulso de calor de ponta simples.

Neste trabalho foi desenvolvido um novo sensor de umidade de solo do tipo pulso de calor de ponta simples, baseado em um único elemento: um transistor bipolar de junção *npn*, que é usado tanto como aquecedor e como sensor de temperatura de alta precisão.

Resultados experimentais, obtidos em medidas realizadas através de uma técnica de interrogação especialmente desenvolvida para este novo sensor mostram que neste trabalho foi possível obter uma sensibilidade cerca de uma ordem de grandeza maior do que nos sensores de pulso de calor com uma ponta e cerca de 20 vezes maior do que nos sensores de pulso de calor de duas pontas.

Outra vantagem da técnica desenvolvida é que o aumento da sensibilidade não é obtido às custas do aumento da corrente drenada da bateria para aquecer o sensor. No sensor desenvolvido é utilizada uma corrente de apenas 6 mA para gerar o aquecimento (com energia dissipada de 1,5 J), enquanto que os sensores de pulso de calor com ponta simples requerem cerca de 50 mA (com 2,4 J de energia dissipada) para operar. Os sensores de pulso de calor de ponta dupla também são fabricados com resistores que requerem cerca de 50 mA para o aquecimento (0.8 J de energia dissipada) para operar corretamente.

Palavras-chave: Sensor de umidade de solo, instrumentação eletrônica, sensor de dissipação térmica, agricultura de precisão.

Abstract

The concern regarding sustainable development and crop inputs optimization (such as water, fertilizers, pesticides and soil PH correction products) has led to the development of the precision agriculture concept, that allows to determine the exact amount of each input required on each ground section (typically one hectare), avoiding waste of inputs.

Low-cost and easily handled soil moisture sensors are very important for allowing a precise irrigation control. The class of sensors which fulfill those requirements are the heat transfer sensors, where there are basically two types of devices: dual (or multi) probe heat pulse sensors and single probe heat pulse sensors.

However, these sensors have a low sensitivity in the most important range of soil humidity θ_v for plants (usually from $5\% \leq \theta_v \leq 35\%$). To cover this 30% soil humidity range with 1% resolution it is necessary to measure temperature with a resolution of 0,026 °C in the dual/multi probe heat pulse sensors and 0,05 °C in the single probe heat pulse sensor.

In this work it was developed a new type of single probe heat pulse sensor, comprised of a single element: an *npn* junction bipolar transistor, that plays the role of both the heating element and a high accuracy temperature sensor.

Experimental results, obtained through an interrogation technique especially developed for this sensor, show a sensitivity about one order of magnitude greater than the typical sensitivity of the single probe heat pulse sensors and 20 times greater than dual probe heat pulse sensors.

Another great advantage of the developed interrogation technique is that the increase in sensibility is not obtained through a higher current being drained from the batteries that power the sensor. The developed sensor operates at a much lower current level than the other sensors, draining only 6 mA from the battery (with an energy of 150 mW). The single probe heat pulse sensor requires 50 mA and 1.5 J of energy to operate, whilst the dual probe heat pulse sensors are manufactured with resistors which also drain 50 mA from the battery with 0.8 J of dissipated energy.

Keywords: Soil Moisture sensor, electronic instrumentation, heat dissipation sensor, precision agriculture.

Acknowledgements

Completing this masters thesis work in the research group of the Department of Electronics and Microelectronics has been a wonderful experience.

First of all, I have to thank my advisor, Prof. Dr. Elnatan Ferreira, for being very supportive during all stages of this work.

It was a great pleasure to work in the DEMIC, where Prof. Elnatan and Prof. Siqueira, both from the Sensors and Electronics Instrumentation research group, established a creative environment where the flow of new ideas (with their associated challenges) promotes intense team work and open collaboration.

The MSc and PhD students of the Sensors and Electronics Instrumentation group in DEMIC comprise a fantastic research group, where everyone benefits from the constant discussions and collaboration.

My most intense collaboration has been with Flávio Morais, who spent hours in my bench work helping me to analyse and debug the first MSP430 code I had ever written.

Luis Duarte (our MSP430 guru) was a great companion and our savior when we simply could not make the MSP430 do what it was supposed to...And also when LabView stubbornly decided to stop receiving the data from my microcontroller.

Filipe Pfrimer helped me with checking my LabView VIs.

Wellington Roque, whose PhD is based on the results of this work, has fabricated all the soil moisture sensors and has also arranged and prepared the material for the experimental work. I hope this work and the developed interrogator will help him in performing a detailed analysis and modeling of this new sensor.

I thank CAPES for providing my funding during the development of this work.

My other colleagues in the DEMIC Sensors and Electronics Instrumentation research group (here cited in alphabetical order) Alcides Cremonesi, Alcino Biazon, Alex Dante, Anderson Spengler, Hugo Bertone, Jefferson Moro, Marcela Koyama and Sérgio Reis were great companions and always had suggestions on how to tackle the difficulties in my experimental work.

Ester Mendes, the secretary of DEMIC, was always kind and efficient, and her support with the paperwork was very important.

Aos meus pais.

“I have yet to see any problem, however complicated, which, when you looked at it the right way, did not become still more complicated.”
Paul Alderson, in *“New Scientist”*, 25 September 1969, 638

Table of Contents

List of Figures	xi
1 Introduction	1
2 Heat Pulse Soil Moisture Sensors	3
2.1 Principle of operation	3
2.2 Dual probe heat pulse sensor	3
2.3 Multi probe heat pulse probe sensor	7
2.4 Single probe heat pulse soil moisture sensors	8
3 A Novel Single Probe Heat Pulse Soil Moisture Sensor	14
3.1 Semiconductors in Single Probe Heat Pulse Sensors	14
3.2 Principle of operation of the single transistor SPHP sensor	15
3.3 Calculating the temperature of a transistor using $V_{BE}(T)$	17
3.4 A simple thermo-electric model of the complete sensor	20
4 Electronic Interrogation System	22
4.1 Principle of operation	22
4.2 Voltage pulse circuit	23
4.2.1 DC-DC converter	24
4.2.2 Voltage pulse generator circuit	25
4.3 Current pulse generator circuit	28
4.3.1 Analog switches	30
4.3.2 The microcontroller and the USB communication circuit	32
5 Characterization of the sensor	36
5.1 Basic functional tests	36
5.2 Application of the sensor in soil moisture measurements	41
5.3 Characterization of the sensor prepared with a 2N2222 transistor	42
5.3.1 Measuring during the heat pulse (2N2222)	42
5.3.2 Measuring before and after the heat pulse (2N2222)	46
5.4 Characterization of the sensor prepared with a BC547 transistor	48
5.4.1 Measuring during the heat pulse (BC547)	48
5.4.2 Measuring before and after the heat pulse (BC547)	51

TABLE OF CONTENTS

x

6 Conclusions

56

Bibliography

59

List of Figures

2.1	Basic schematic of a heat pulse dual probe sensor.	4
2.2	Curve of ΔT_m as a function of θ_v for the S_0 dual probe heat pulse sensor.	5
2.3	Variation of ΔT_m as a function of the distance between the probes r	6
2.4	Error in the measurement of ΔT_m as a function of small variations of the distance between the probes Δr for different values of r	7
2.5	Multiprobe heat pulse soil moisture sensor.	8
2.6	Example of a single probe heat pulse sensor encapsulated in porous ceramic.	9
2.7	TMAS soil moisture sensors.	9
2.8	Example of heat dissipation sensor responses.	10
2.9	Heat transfer across a composite slab: electrical equivalent model.	11
2.10	Equivalent model of the heating probe.	11
2.11	Steady-state temperature profile inside the epoxy for a heat pulse of 80 mW.	12
3.1	Basic schematic of the V_{BE} measuring points and the pulse heating application.	15
3.2	Basic thermal model of the 2N2222 transistor.	16
3.3	Comparison of measured results with the thermal simulation of a SPHP sensor made with 2N2222 transistor in air.	16
3.4	Simulation result for the thermal simulation of a SPHP sensor made with a 2N2222 transistor, for different heatsink materials.	17
3.5	Non-linearity of $V_{BE}(T)$ as a function the temperature.	18
3.6	Complete thermo-electrical model of the sensor.	20
3.7	Simulated results of $V_{BE}(t)$ for the same heat pulse applied, when two distinct heatsink materials are in contact with the sensor.	21
4.1	Block diagram of the electronic interrogator	23
4.2	Simplified internal block diagram of the LTC1144 switched-capacitor dc-dc converter	25
4.3	Simplified schematic of the voltage pulse circuit	26
4.4	Measured result in the output of the dc-dc converter and voltage regulator.	27
4.5	Measured result of the voltage pulse in the output of the op-amp.	28
4.6	Block diagram of the current pulse generator circuit	28
4.7	Block diagram of the current pulse generator circuit	29
4.8	Measured result of the current pulse generator circuit	30
4.9	Schematic diagram of clock conditioning circuit for the analog switches and ± 9 V and ± 2.5 V power supplies	31

4.10	Measured result in the output of the op-amp (clock signal of the ADG819 switches).	31
4.11	Schematic diagram of the microcontroller and USB circuits	32
4.12	Measurement of a constant V_{BE} voltage, showing that a low-noise circuit was achieved	33
4.13	Complete schematic of the developed interrogator	34
4.14	Layout of the double-layer PCB designed for the interrogator	35
5.1	Labview plot of the measured V_{BE} , showing the three phases of measurement.	37
5.2	Plot of the measured V_{BE} of a sensor prepared with a 2N2222 transistor in air and inserted in a dry soil.	37
5.3	Plot of the calculated temperature in the sensor, from $V_{BE}(T)$ measurements presented in Fig. 5.2.	38
5.4	Plot of the calculate temperature in the sensor, from $V_{BE}(T)$ measurements, after proposed temperature correction.	39
5.5	Measured result of 2N2222 transistor immersed water.	41
5.6	Measured result of a sensor prepared with a 2N2222 transistor for different values of θ_v	43
5.7	Plot of the temperature difference ΔT as a function of soil water content θ_v for a sensor prepared with a 2N222 transistor.	43
5.8	Comparison of the measured temperature difference ΔT as a function of soil water content θ_v for three different sensors: Campbell 229 SPHP commercial sensor, a DPHP sensor presented by Mori <i>et al.</i> and the developed sensor prepared with a 2N2222 transistor.	44
5.9	Plot of the thermal conductivity of three types of soil: loam, quartz sand and organic	45
5.10	Effect of density and water content on thermal resistivity of a loam soil. The bulk densities are 1.06 Mg/m ³ for void ratio of 1.5, 1.33 Mg/m ³ for void ratio 1, and 1.59 Mg/m ³ for void ratio of 0.67.	45
5.11	Measured variation of ΔT (before and after the heat pulse) for various values of θ_v , as a function of the time.	46
5.12	Measured variation of ΔT (before and after the heat pulse) for each measurement point position, various values of θ_v	47
5.13	Measured variation of ΔT (before and after the heat pulse) for point No. 3 and point No. 8, for various values of θ_v	48
5.14	Measured variation of ΔT in the sensor prepared with a BC547 transistor in the air and into a dry soil.	49
5.15	Measured variation of ΔT in the sensor prepared with a BC547 transistor immersed in water.	50
5.16	Measured variation of ΔT as a function of the time, for the sensor prepared with a BC547 with various θ_v	50
5.17	Measured variation of ΔT in the sensor prepared with a BC547 transistor as a function of θ_v	51
5.18	Measured variation of ΔT (before and after the heat pulse) for each measurement point position, various values of θ_v (BC547).	52
5.19	Measured variation of ΔT (before and after the heat pulse) for measured points in position No.3 and No.8, as a function of θ_v (BC547).	53

5.20	Measured variation of ΔT (during the heat pulse) for three values of θ_v , as a function of the time (2N2222).	54
5.21	Measured variation of ΔT (during the heat pulse) for three values of θ_v , as a function of the time (BC547).	55

Chapter 1

Introduction

THE classic study conducted by Nielsen et al [1] in 1973, which investigated the spatial variability of soil-water properties for a 150 ha field at the University of California's West Side Field Station in the San Joaquin Valley, showed that a large variation of the soil physicochemical properties can be found, and this spatial variability creates non-homogeneous results in the crop's productivity.

The rudimentary concept of precision agriculture concept appeared in the beginning of the 1980s in the United States, when the input of fertilizers in the crop fields were varied and the harvest results were monitored, in order to find the optimal amount of fertilizer which had to be applied to each region of the soil [2]. This introduced the concept of variable rate technology for the application of inputs. On the other hand, the effective variable rate application of inputs required the use of a grid to divide the crop regions, and at the same time the concept of grid sampling (one sample per hectare) appeared.

The characterization of soil spatial variability is fundamental to create the recommendation for site-specific crop management, and this site-specific crop management (both in what concerns irrigation, fertilization and pesticide application) is known as precision agriculture. Because large variations of landscape and soil properties can be found in small areas of land, sometimes grids as small as 20 m x 20 m are necessary to determine the correct inputs for a crop [3].

Efficient management of irrigation systems requires the implementation of precision agriculture techniques. In precision agriculture, the grid sampling of the crop fields produces accurate data for controlling and optimizing the amount of inputs (water, fertilizers, pesticides, PH correction products) to be used in each grid region, reducing both the production costs and the environmental impacts. This practice leads to a high yield sustainable production practice that can assure a long term food supply under the optimal ecological, economic and social conditions.

In order to implement the precision agriculture techniques for irrigation management, the use of reliable and accurate soil moisture sensors is mandatory. Today, a large number of sensors, based on heat transfer [4], electromagnetic [5], tensiometric [6], nuclear [7], capacitance [8] and resistance [9] techniques are available for measuring soil moisture. Although many of the sensors fabricated using those techniques present good accuracy, most of them are suited only for laboratory use, since they are very expensive and/or are not practical to be used in real applications in crop fields.

The sensors which are the most adequate for use in crop fields are those based on the heat transfer principle. The reason for this success is that heat transfer sensors are usually small, low-cost, and can be easily applied in the fields. However, all of the techniques available present low sensitivity, and

high resolution measurements can only be obtained if sophisticated interrogators are used. Besides this problem, in the humidity range where the plants require a very precise control of irrigation, the sensitivities of the available sensors are very poor.

This low sensitivity jeopardizes the efficiency of the precision agriculture techniques. For example, if the sensors indicate that the amount of moisture in the soil is near the lower limit (the water content in the soil *seems* to be enough to leave the plants one extra day without irrigation), since this information is known to be not very accurate, the farmer will not take any risk and will irrigate his crop. In a large plantation this can result in a enormous waste of water, especially if a substantial rain falls on the next day.

The purpose of this research is to present a new heat transfer soil moisture sensor and also develop a precision electronic interrogator for this new soil moisture sensor. The sensor is based on a single very low-cost npn bipolar transistor. Experimental results of the application of the new sensor in laboratory soil moisture measurements with the interrogation equipment developed will be presented, showing that both the developed sensor and the electronic interrogation technique used can provide accurate and much better sensitivity than today's available soil moisture sensors.

Chapter 2

Heat Pulse Soil Moisture Sensors

2.1 Principle of operation

THE principle of operation of the heat pulse soil moisture sensors is based on the variation of the thermal conductivity of a porous material. The porous material can be a porous block (e.g., made of gypsum or ceramic) or the soil itself. The porous material's thermal conductivity is changed by the amount of water absorbed into its pores and, therefore, its heat transfer properties change with the amount of water. By applying a controlled amount of heat in the center of the sensor and measuring its temperature (which depends on the thermal conductivity of the surrounding material) it is possible to relate the measured temperature with the amount of water absorbed in the soil.

There are three types of heat pulse soil moisture sensors: the dual probe heat pulse (DPHP), the multiprobe heat pulse sensor (MPHP), and the single probe heat pulse (SPHP). Each type presents its advantages and disadvantages, and a detailed explanation of the three types of sensors will be presented in next sections.

2.2 Dual probe heat pulse sensor

The dual probe heat pulse sensors are comprised of two probes, mounted at a fixed distance (usually 6 mm), with one heating element in one probe and one temperature sensing element in the other probe. The heating element is always a NiCr wire wound resistor and the temperature sensing element can be a thermocouple, a thermistor or an integrated circuit designed for temperature measurement. Figure 2.1 shows the basic schematic of a dual probe sensor.

To make a soil moisture measurement with these sensors, first a heat pulse is applied to the heating element during a fixed period of time t_m . The energy of the heat pulse depends on the controlled current I_0 that is forced in the NiCr resistor R_0 , so that the energy dissipated in the heating element is given by:

$$W_m = (R_0 I_0^2) \cdot t_m \quad (2.1)$$

The heat pulse travels through the soil, and the maximum temperature reached in the sensing element is measured. The higher the water content in the soil the better it dissipates the heat and,

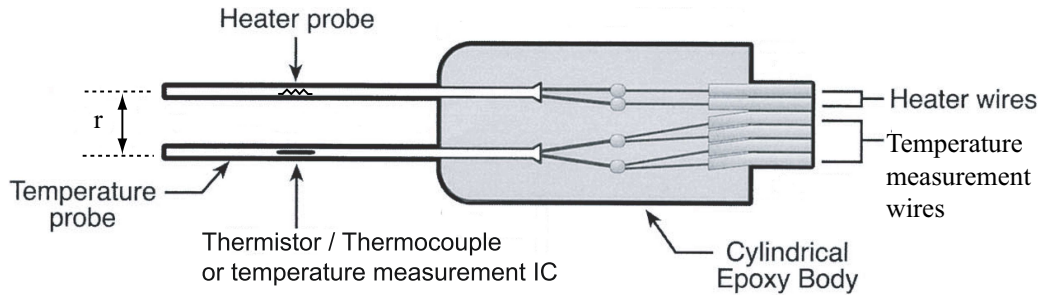


Fig. 2.1: Basic schematic of a heat pulse dual probe sensor.

therefore, the temperature peak sensed by the second probe decreases as the water content in the soil increases.

Consequently, after a calibration procedure, the amount of water in the soil can be determined by measuring the maximum temperature reached on the second probe (the sensing element). The relationship that describes the temperature increase ΔT_m in a sensing element located at a distance r of a heating element, as a function of the heat energy q and the water content θ_v in the soil, developed by [10], is presented in Eq. 2.2.

$$\Delta T_m = \frac{q}{e\pi r^2(1.92X_m + 2.5X_o + 4.18\theta_v)} \quad (2.2)$$

where q is the quantity of heat liberated per unit length of heater (in $\text{J} \cdot \text{m}^{-1}$), e is the base of the natural logarithm, X_m , X_o are, respectively, the volumetric fractions of mineral and organic contents of the soil [11], and θ_v is the volumetric fraction of water in the soil. In soils with low organic content the term X_o is neglected [12]. The coefficients 1.92, 2.5 and 4.18 are given in $\text{MJ} \cdot \text{m}^{-1} \cdot ^\circ\text{C}^{-1}$.

The volumetric fraction of the water in the soil θ_v , given in $\text{m}^3 \cdot \text{m}^{-3}$, is defined by the ratio between the volume of water and the volume of dry soil in the region under measurement, and is usually expressed in percentages. For example, if 100 ml of dry soil is hydrated with 30 ml of water, it is said that the resulting soil has a volumetric humidity of 30%.

It is important to notice that Eq. 2.2 was determined using not only heat transfer theory, but through exhaustive experimental measurement and data fitting [10, 13], and can be used in any type of soil. To study the behaviour of a dual probe heat pulse sensor, an hypothetical sensor S_0 with the following typical parameters will be used: $q = 600 \text{ J} \cdot \text{m}^{-1}$, $X_o = 0$, $X_c = 0,54$, $r = 6 \text{ mm}$.

A plot of Eq. 2.2 for sensor S_0 is presented in Fig. 2.2, where it can be seen that the maximum temperature ΔT_m decreases as θ_v increases. The value of the full scale variation of ΔT_m is small: $\Delta T_m \approx 1.5^\circ\text{C}$ for $0\% \leq \theta_v \leq 100\%$. When the soil moisture varies in a typical agricultural range of 5% ($\Delta T_m = 1.6^\circ\text{C}$) to 35% ($\Delta T_m \approx 0.8^\circ\text{C}$), the variation in θ_v is approximately 0.8°C . Consequently, this type of sensor is very difficult to be read accurately, since to detect a change of 1% in soil moisture in the agricultural range it is necessary to measure ΔT_m with a resolution of approximately 0.026°C .

Due to the trade-offs involving sensitivity, power dissipation and mechanical properties, overcoming the sensitivity limitations of dual probe heat pulse sensor is not an easy task. These compromises become evident when the sensor's sensitivity is analyzed. To calculate the sensitivity φ of this sensor, one must take the partial derivative of ΔT_m with respect to θ_v , which is given by:

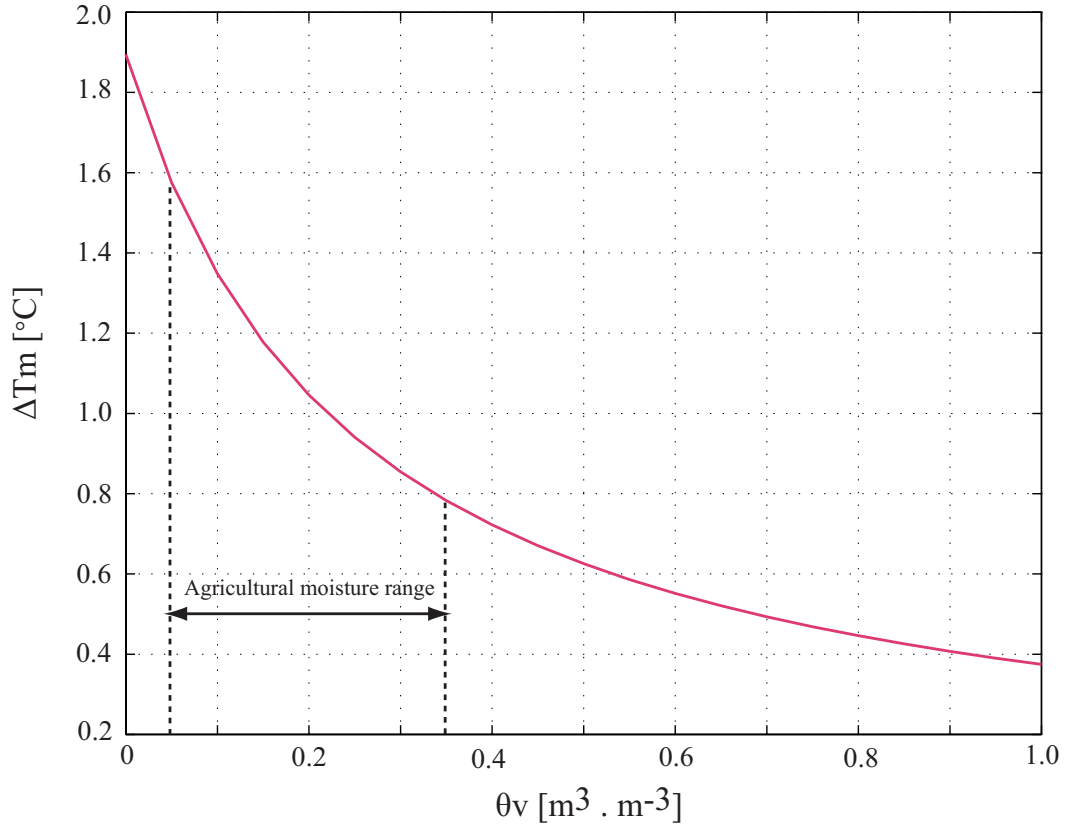


Fig. 2.2: Curve of ΔT_m as a function of θ_v for the S_0 dual probe heat pulse sensor.

$$\varphi = \frac{\delta \Delta T_m}{\delta \theta_v} = \frac{-4.18q}{e\pi r^2(1.92X_m + 2.5X_0 + 4.18\theta_v)^2} \quad (2.3)$$

Examining Eq. 2.3 one concludes that to increase the sensitivity φ it is necessary to: (a) increase the energy dissipated q ; or (b) decrease the distance r between the probes.

As can be easily noted in Eq. 2.3, the sensitivity increases linearly with the energy of the heat pulse. However, since the interrogators must be battery operated to be employed in the field, increasing significantly the energy is obviously not a feasible option.

Reducing the distance between probes seems to be a more interesting solution, because the sensitivity φ is proportional to $1/r^2$. A plot of the sensitivity of sensor S_0 for $r = 6$ mm, $r = 5$ mm, $r = 4$ mm and $r = 3$ mm, presented in Fig. 2.3, shows that, when the value of r is reduced from 6 mm to 3 mm, an increase of more than 4 times is obtained in the the full scale variation of ΔT_m (from $\approx 1.5^\circ\text{C}$ to $\approx 7.0^\circ\text{C}$).

On the other hand, due to mechanical problems that a sensor with a short distance between probes can present (in the construction of the probe or during its application in the field), it is necessary to investigate the sensitivity of ΔT_m to variations in r .

Taking the partial derivative of ΔT_m with respect to r , one obtains:

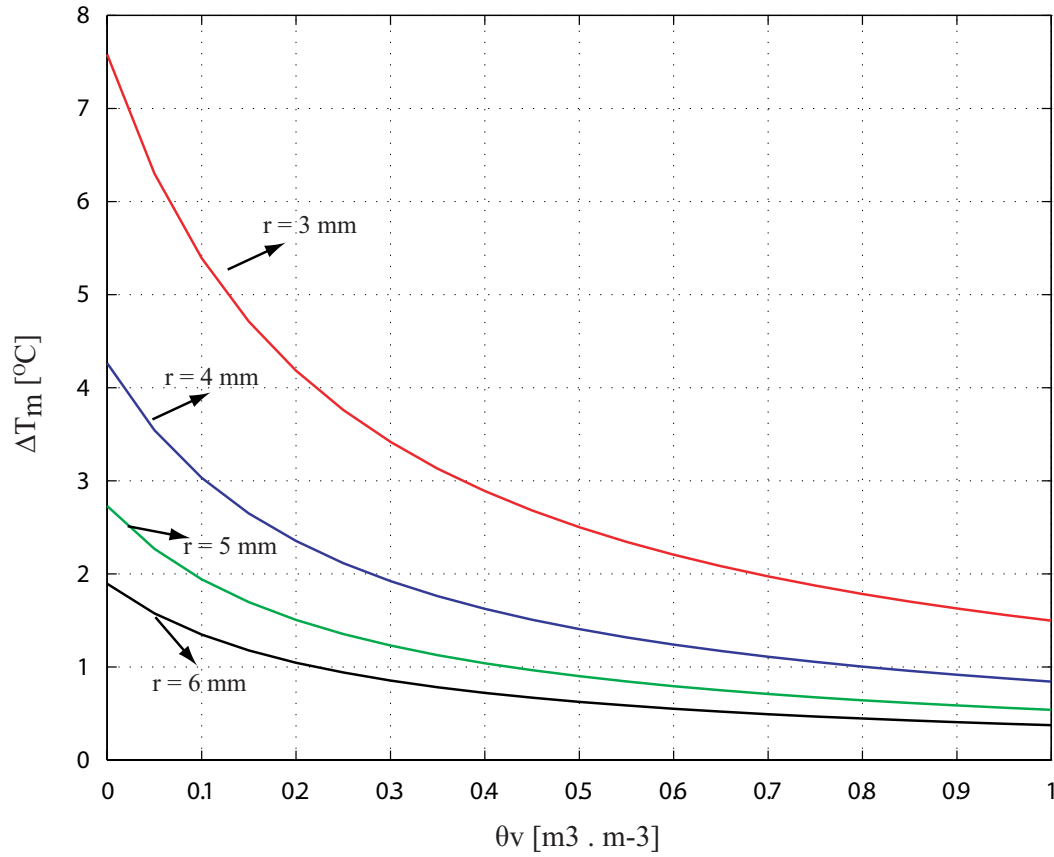


Fig. 2.3: Variation of ΔT_m as a function of the distance between the probes r .

$$\psi = \frac{\delta \Delta T_m}{\delta r} = \frac{-q}{2e\pi r^3(1.92X_m + 2.5X_0 + 4.18\theta_v)^2} \quad (2.4)$$

Observing Eq. 2.4 one concludes that, as expected, the sensitivity of ΔT_m with respect to the variations in the distance between the probes r increases rapidly as r decreases, due to the r^3 term in the denominator. Unfortunately, this characteristic imposes a severe limitation on the minimum value of r that the designer can use to fabricate a sensor. The problem is that undesired variations of r , due to a fabrication inaccuracy or caused by small deflections in the probes (a common problem when the sensors are inserted into the soil), will cause a variation in the sensitivity of the sensor.

For the sensor S_0 , the measured value of ΔT_m as a function of θ , for small deviations of Δr for nominal values of r were calculated and the results are plotted in Fig. 2.4. Thus, although it has been shown in Fig. 2.3 that reducing the distance between the probes to $r = 3$ mm the full scale increased to $\approx 7.0^\circ\text{C}$, a deflection of only $300 \mu\text{m}$ in the probes results in an ΔT_m error of approximately 2.0°C for $\theta_v = 5\%$, or circa of 28.5 % of the sensor's full scale.

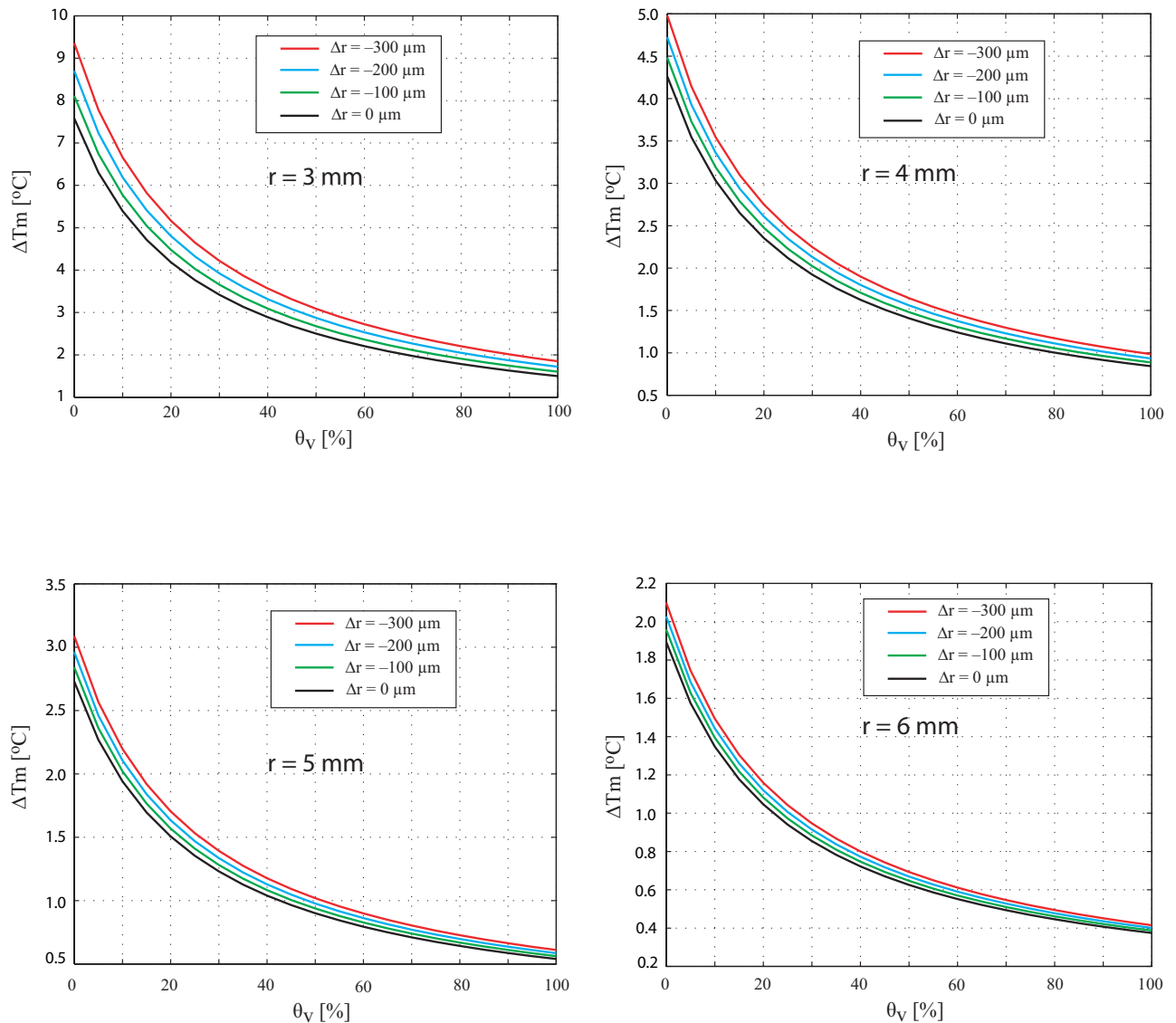


Fig. 2.4: Error in the measurement of ΔT_m as a function of small variations of the distance between the probes Δr for different values of r .

2.3 Multi probe heat pulse probe sensor

To overcome this severe limitation of the DPHP sensors, some authors have proposed the fabrication of multi-probe sensors [14–16], with one central heating element and 4 (or more) sensing elements evenly distributed around the heating element, as shown in Fig. 2.5. By making an average of the readings of the 4 elements, the errors due to bending/deflection of the probes during application in the soil or even during construction can be somewhat minimized. However, the cost of the sensor increases dramatically, since the most expensive component in the sensor is the temperature sensing element (thermocouple or thermistor). Besides this cost limitation, the sensor's calibration procedure is very time-consuming because all temperature sensing elements must be calibrated individually.

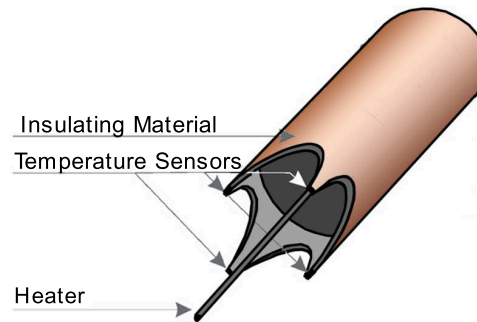


Fig. 2.5: Multiprobe heat pulse soil moisture sensor.

2.4 Single probe heat pulse soil moisture sensors

The third type of heat pulse soil moisture sensor is the single probe heat pulse (SPHP). It operates on similar principles of the dual and multi probe sensors, however, the heating and sensing element are encapsulated in the same probe. The heating and sensing elements are mounted together, as close as possible, and instead of measuring the maximum temperature reached at a fixed distance from the heater, a long heat pulse is applied (typically 20 – 30 s) and the temperature of the heating element is measured just before the heat source is turned-off.

There are basically two techniques for the manufacturing single probe heat pulse sensors. In one of the fabrication techniques both the heating and sensing element are encapsulated inside a very high thermal conductive material, for example a stainless steel needle. Both the sensor and the heating element must be placed as close as possible. To achieve a good path with low thermal resistivity between the two elements, the needle is filled with a thermal conductive epoxy and the the needle is encapsulated inside a porous block, like gypsum or ceramic. A schematic drawing of a ceramic single probe heat pulse sensor is presented in Fig. 2.6.

In the other technique, which is being used to evaluate soil moisture in space flight applications, the heating and sensing elements are encapsulated, also very close one to the other, inside a very small and thin thermal conductive resin epoxy coating. There is no ceramic involving the epoxy case, so the porous material is the soil itself. These very small and lightweight sensors (7.6 mm x 2.5 mm), called TMAS, are being developed and evaluated to be used in the automated grow of plants in microgravity environment, in future long-term self-sustainable space missions. A photograph of the TMAS sensors produced by Orbital Technologies Inc. [17], [18] is presented in Fig. 2.7.

The SPHP sensor usually presents a higher sensitivity when compared to the dual probe design, as we can see in Fig. 2.8, where a curve from a sensor manufactured by Campbell [4] is presented, and a full scale of approximately 2.3°C in the range of $0\% \leq \theta_v \leq 100\%$ is observed. For the agricultural range of 5 – 35%, a variation of $\approx 1.5^{\circ}\text{C}$ is obtained, showing that it is necessary to measure the temperature with a resolution of 0.05°C if it is desired to detect a 1% variation in θ_v .

This is almost twice the 0.8°C variation found in the agricultural range of a dual probe heat pulse sensor, but it is obtained by using a higher energy to heat the probe. This happens because although the power dissipated in the heating element is about the same used in the DPHP sensors (85 mW),

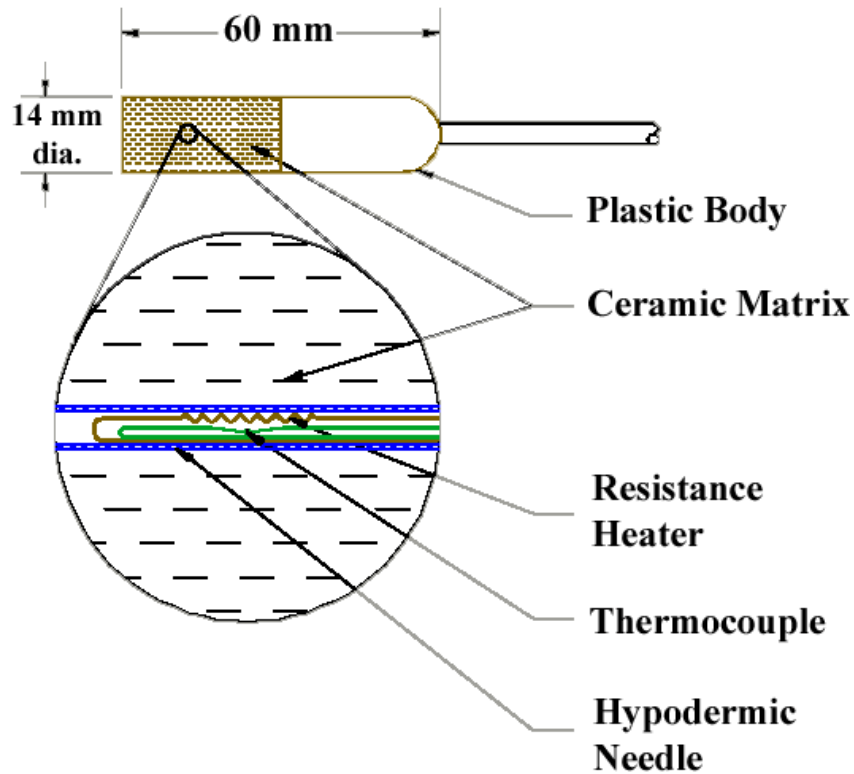


Fig. 2.6: Example of a single probe heat pulse sensor encapsulated in porous ceramic.

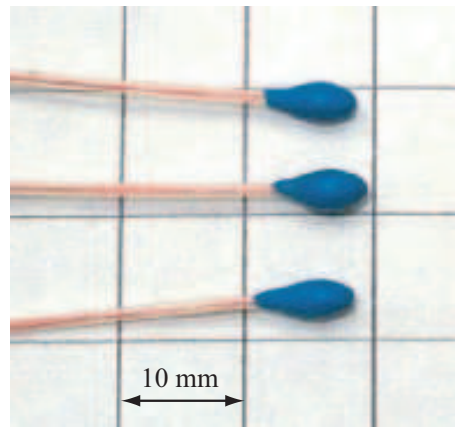


Fig. 2.7: TMAS soil moisture sensors.

the time required to make a measurement is longer (usually 30 s), whilst for the dual probe sensor it is approximately 8-10 s. The energy dissipated in the SPHP sensors is about 2.5 J.

Analogous to the DPHP sensor, variations in the distance between the heating element and the sensing element result in different behavior of the fabricated sensors. However, this sensitivity to the variation in the distance between the probes is smaller because the material which encapsulates the

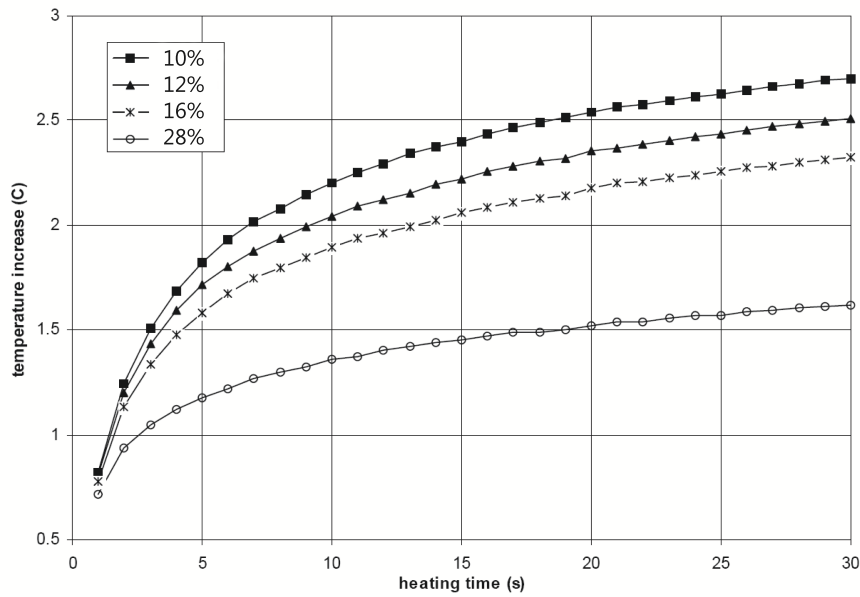


Fig. 2.8: Example of heat dissipation sensor responses.

heating and the sensing probes is an epoxy with a low thermal resistance. Although it is expected that the dispersion in the sensitivity is smaller than in the DPHP sensor, it is worth to evaluate the thermal behavior of this type of sensor in order to investigate the errors induced by these variations.

To calculate the temperature distribution in the epoxy, the conventional equivalent electric model of a one-dimensional heat conduction system (shown in Fig. 2.9) will be used, where a slab of material is heated on the left end by a heat source and the right end is embedded in an environment assumed to be at a constant temperature T_A .

In this model the equivalent of the heat transfer rate \dot{Q} is the current, the equivalent of the temperature difference $T_i - T_{i+1}$ is the voltage drop $V_i - V_{i+1}$ and the thermal resistance of the material R_{THi} is defined from the expression:

$$\dot{Q} = \frac{T_i - T_{i+1}}{R_{THi}} \quad (2.5)$$

The thermal resistance of each portion of the material is a function of the thermal conductivity λ_i , the length L_i and the the area A , and is written as:

$$R_{THi} = \frac{L_i}{\lambda_i A} \quad (2.6)$$

The capacitors C_i , given in $\text{J} \cdot \text{m}^{-3} \cdot ^\circ\text{C}^{-1}$, are equivalent to the thermal capacity of the materials. It is worth to notice that the capacitors are used only in transient analysis. The temperature analysis in steady-state conditions is equivalent to a DC analysis of the circuit, and the capacitors are ignored.

To calculate the importance of the relative position of the heating and sensing elements, it is necessary to study the heat transfer inside the epoxy wall, and thus only one thermal resistance R_{TH} (which value depends on the distance between the probes L) will be considered. The model is shown in Fig. 2.10.

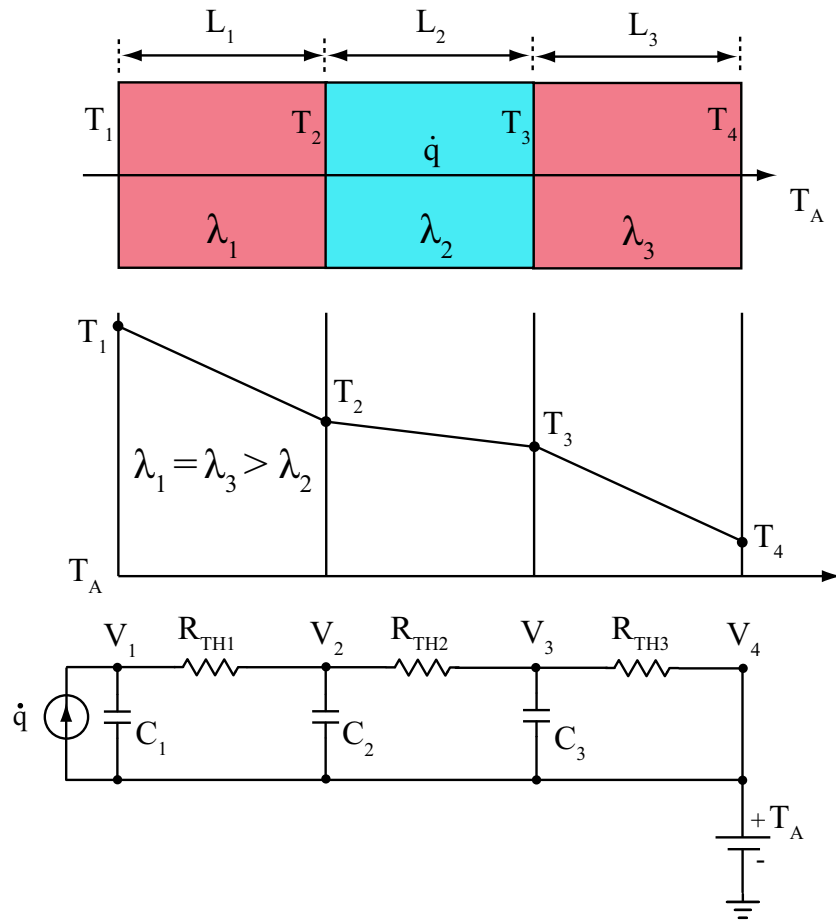


Fig. 2.9: Heat transfer across a composite slab: electrical equivalent model.

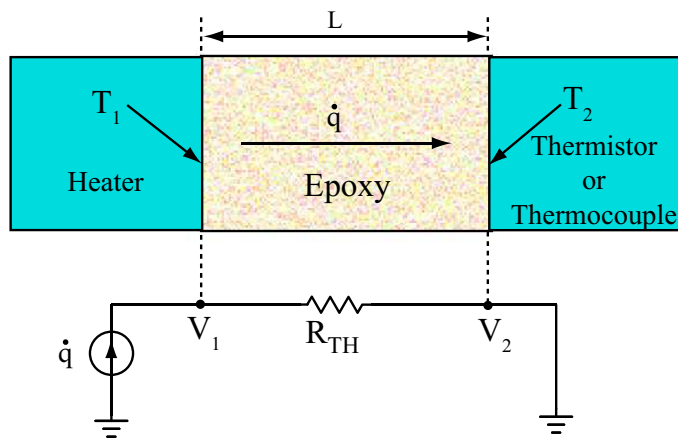


Fig. 2.10: Equivalent model of the heating probe.

Ham *et al* [19] showed that an adequate material to manufacture a heat pulse sensor is the urethane epoxy CR600, because it presents good electrical insulation and a good thermal conductivity ($\lambda_{TH} =$

$0.2 \text{ W} \cdot \text{m}^{-1} \cdot ^\circ\text{C}^{-1}$). Thus, for this epoxy, considering a section with area A , the thermal resistance R_{TH} can be written as:

$$R_{TH} = \frac{L}{A \cdot 0.2 \frac{\text{W}}{\text{m}^\circ\text{C}}} = \frac{5L}{A} \cdot \frac{\text{m}^\circ\text{C}}{\text{W}} \quad (2.7)$$

Thus, with the heat flux defined by $\dot{q} = \dot{Q}/A$ it is possible to write:

$$\dot{q} = \frac{T_1 - T_2}{A \cdot 5L} \quad (2.8)$$

Using a heat pulse of 80 mW ($\dot{q} = 80 \text{ mA}$), it is possible to calculate the temperature difference between the heating and sensing elements caused by the losses in the epoxy as:

$$T_1 - T_2 = 80 \text{ mW} \cdot 5(L) = 0.4 L \quad (2.9)$$

A plot of temperature inside the epoxy (from T_1 to T_2) as a function of L is presented in Fig. 2.11. The maximum value considered for L was 1 mm because the hypodermic needle that is used to encase the sensing/heating elements has an internal diameter of 1.1 mm. Thus, it is reasonable to estimate that the maximum manufacturing error Δr is less than 0.3 mm. With $\Delta r = \pm 0.3 \text{ mm}$, a dispersion error of approximately $\pm 120 \mu^\circ\text{C}$ shall be present in the fabricated sensors, which represents an error of only 0.008% in the full agricultural range of 1.5°C , and can be neglected.

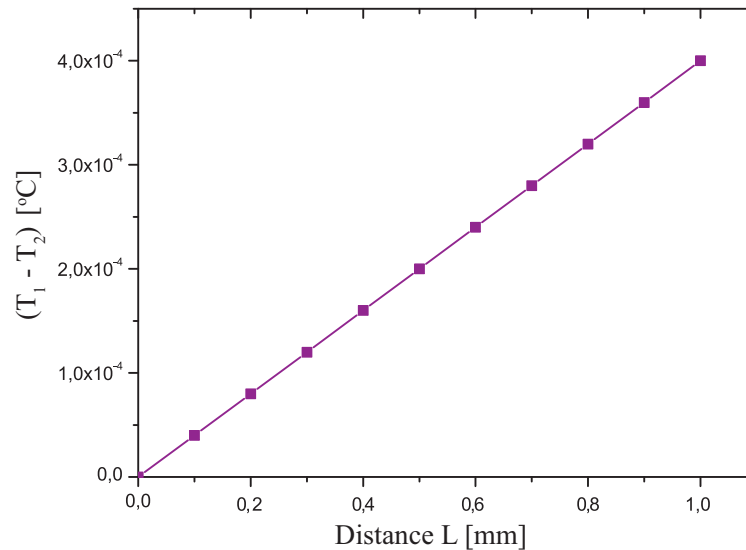


Fig. 2.11: Steady-state temperature profile inside the epoxy for a heat pulse of 80 mW.

This result indicates that SPHP sensors presents a higher sensitivity with respect to the soil moisture variation and are less dependent on the manufacturing process. However, for achieving low cost it is necessary to use thermistors as the temperature sensing elements, and a calibration procedure for the thermistor is mandatory. When the SPHP sensors are manufactured with a thermocouple, the calibration may be skipped but the cost of the sensor increases typically one order of magnitude.

In next Chapters a novel type of single probe heat pulse sensor, with only one device (that works as both heating and temperature sensing elements) will be proposed, designed and evaluated [20]. A

novel interrogation technique will also be developed and the electronics circuits that implement the interrogation technique will be designed, fabricated and tested.

Chapter 3

A Novel Single Probe Heat Pulse Soil Moisture Sensor

3.1 Semiconductors in Single Probe Heat Pulse Sensors

ALTHOUGH, as shown in Chapter 2, SPHP sensors still require individual calibration after assembly, they present a sensitivity which is typically twice higher than the DPHP sensors, and it is worth to investigate novel techniques aiming at the improvement of this type of sensors regarding its sensitivity and fabrication process. If the sensors are intended to be used in space flight applications, weight and size are also a very important concern.

The first idea of using a semiconductor pn junction as the temperature sensing element in soil moisture sensors was presented by Phene *et al.* in 1971 [21] where a NiCr wire wrapped around a diode was encased in a porous block. Many modern techniques use semiconductor ICs to measure temperature [14, 22], and those sensors use two separate elements: the silicon-based temperature measuring device and a NiCr resistor as the heating device.

In this work a completely novel approach was used to employ a nnp transistor in a SPHP soil moisture sensor. A pn junction (the base-to-emitter junction of a bipolar transistor) will be used to measure the temperature and, instead of using another element to heat the semiconductor, the other junction of the transistor (base-to-collector) will be externally controlled to heat the whole device.

The power dissipated (P_D) in a bipolar transistor is given by the very well-known equation:

$$P_D = I_C V_{CE} + I_b V_{BE} \quad (3.1)$$

where the second term ($I_b V_{BE}$) can usually be neglected, since $I_b \ll I_C$.

Thus, to increase the dissipated power in a transistor, it is very interesting to simultaneously increase the collector current I_C and the collector-to-emitter voltage V_{CE} . This is especially important if it is desired to obtain a high power with a low current. Hence, for the same current applied, if the V_{CE} is increased by a factor of 20 (e.g., from 1 V to 20 V), the power dissipated in the transistor would be increased by a factor of 20.

All available DPHP and SPHP sensors use currents in the order of 50 mA to dissipate a power of 80 mW. To illustrate the importance of this technique for using small currents for the power dissipation, in a transistor with $V_{CE} = 30$ V, it will be necessary only 2.67 mA to dissipate the same 80 mW

power. Reducing the current makes the sensor more adequate to be used with portable interrogation devices, which are always powered by batteries.

Furthermore, the discrete bipolar transistor is probably the most well known semiconductor device. Its fabrication process has been well dominated for decades, both electrical and thermal parameters are very well modeled, it is small, lightweight and has a very low cost (about US\$ 0.03). The metal can body of a 2N2222 transistor measures 4.9 mm x 5.3 mm (about the same dimensions of the TMS) and weights less than 1 g. Consequently, if a SPHP sensor can be implemented using a single off-the-shelf standard transistor, it is a strong candidate to be used not only in field crop monitoring but also in space flight applications.

3.2 Principle of operation of the single transistor SPHP sensor

The complete sensor consists solely of a transistor. Before the heat pulse, the transistor is biased at a low current and low voltage level (I_{Ci}, V_{CBi}). A heat pulse is then applied to the transistor, by simultaneously increasing the collector current to I_{Cm} and the collector-to-base voltage to V_{CBm} . After a heat pulse with duration $t_f - t_i$, both the current and voltage return to their initial values I_{Ci} and V_{CBi} . The value of V_{BE} is measured before and after the heat pulse, and the difference ΔV_{BE} is used to calculate the temperature variation in the transistor. The diagram of the measurement points and pulse heat application technique is presented in Fig. 3.1

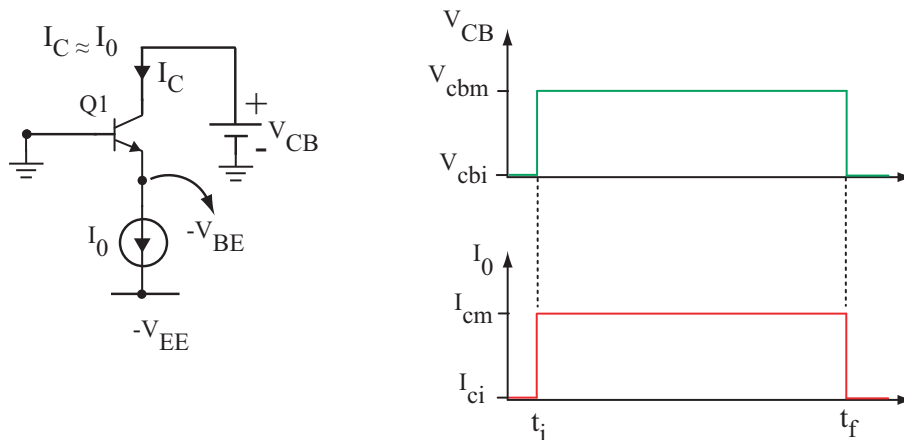


Fig. 3.1: Basic schematic of the V_{BE} measuring points and the pulse heating application.

As mentioned in Chapter 2, the soil's thermal conductivity changes with the volumetric content of water. Since, for a given dissipation power, the temperature increase in a transistor package depends on the thermal conduction process between the package and the heatsink material, inserting the transistor directly into the soil shall result in a system that has a response similar to the conventional two-elements SPHP soil moisture sensors.

To verify the feasibility of this new technique, the thermal-electric behavior of a transistor was simulated in LTSPICE [23]. The temperature increase in the transistor was simulated using the thermal model presented in [24], where it is shown that for $t > 100\mu s$ a one time constant model is

adequate to represent the thermal characteristics of a transistor/heatsink system. The model used is presented in Fig. 3.2.

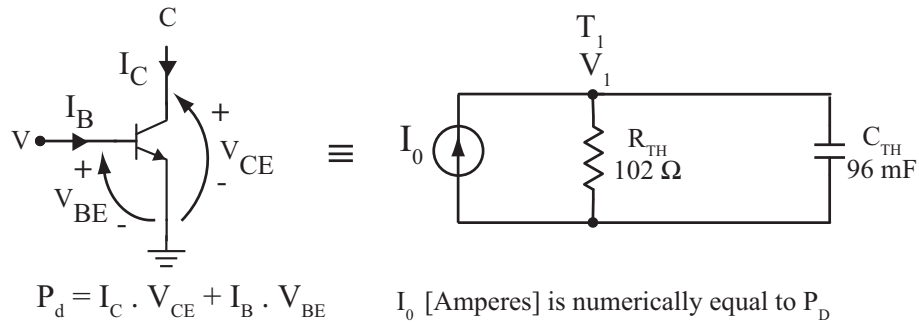


Fig. 3.2: Basic thermal model of the 2N2222 transistor.

The first simulation was ran to verify the expected temperature increase in the transistor in the air. The values of the thermal resistance and thermal capacitance were adjusted to fit the experimental data measured on a 2N2222 transistor. The LTSPICE simulation was performed with I_0 set as a pulse with duration of 10 s and amplitude of 150 mA (for $I_C = 6$ mA and $V_{CB} = 25$ V and neglecting the power dissipation caused by the base current, one has $P_D \approx 150$ mW).

The comparison of the simulated results with the measured data is presented in Fig. 3.3.

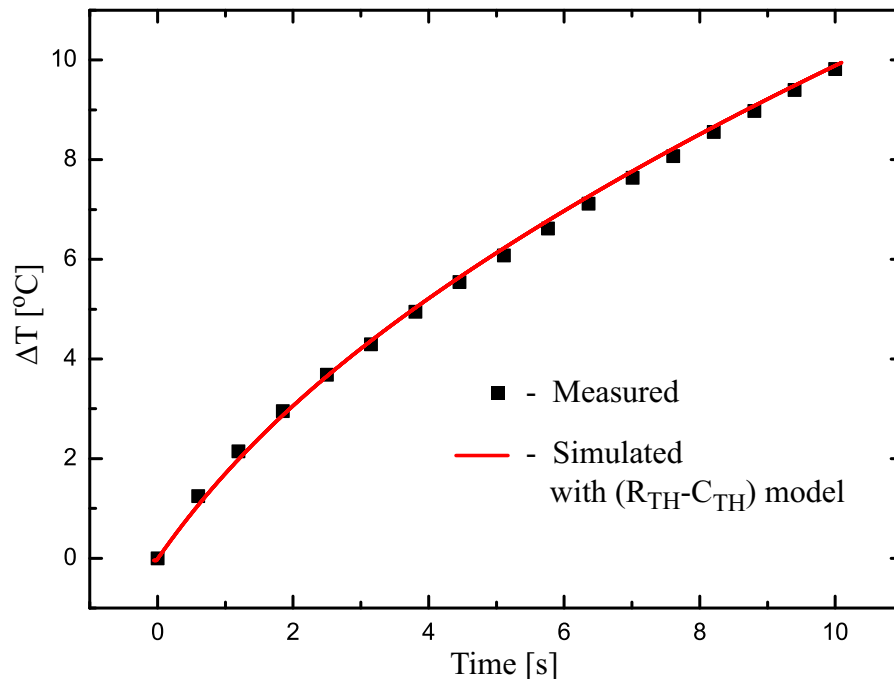


Fig. 3.3: Comparison of measured results with the thermal simulation of a SPHP sensor made with 2N2222 transistor in air.

As it can be seen, the simulated results using $R_{TH} = 102\Omega$ and $C_{TH} = 96$ mF are in good agreement with the measured thermal characteristics of the transistor.

Since the electrical model is very simple and the solution of the voltage $V_1(t)$ in the circuit of Fig. 3.2 is:

$$V_1(T) = (I_0 R_{TH}) \left[1 - \exp\left(-\frac{t}{R_{TH} C_{TH}}\right) \right] \quad (3.2)$$

it is expected that the thermal behavior of the sensors can be easily predicted by using this simple electrical model.

The same circuit was simulated with a heatsink material which has a lower thermal resistance $R_{TH2} = R_{TH}/2 = 51\Omega$ and a higher thermal capacitance $C_{TH2} = 2C_{TH} = 192\text{mF}$, to verify the change in temperature variation when a material with a different thermal characteristics is in contact with the transistor's case. The result of both simulations is presented in Fig. 3.4.

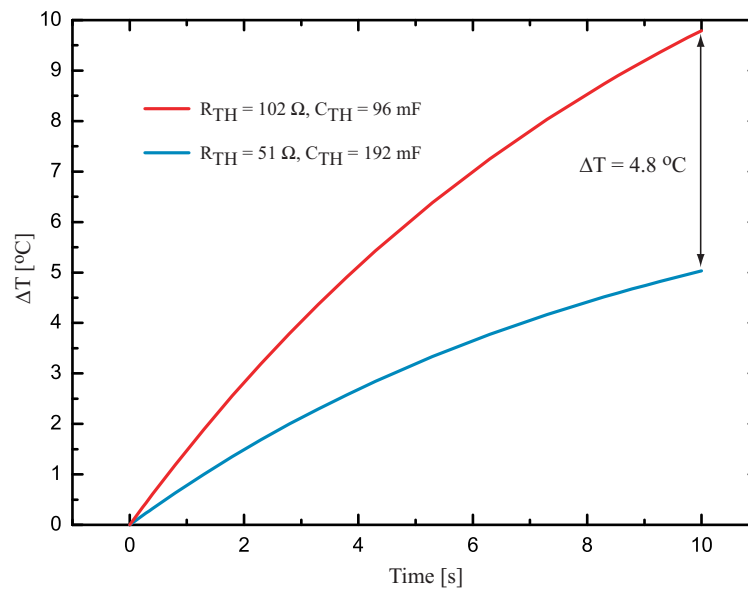


Fig. 3.4: Simulation result for the thermal simulation of a SPHP sensor made with a 2N2222 transistor, for different heatsink materials.

As it can be seen from the simulations, at the end of the heat pulse it is observed that a $\Delta T = 4.8^\circ\text{C}$ is found between the two cases. Since, for θ_v varying in the range of 5% to 35% both the conductivity and thermal capacity of the soil presents a variation similar to those used in this simulation [25], it is expected that similar values of ΔT will be found in sensors fabricated using this new technique.

3.3 Calculating the temperature of a transistor using $V_{BE}(T)$

The accurate knowledge of the variation of V_{BE} as a function of the temperature is the basis for the design of all bipolar voltage references and temperature sensors. For a transistor with a collector current given by $I_C = AT^m$ where A is a constant (e.g., if $m = 0$ the collector current is independent of the temperature), the expression that describes V_{BE} as a function of the temperature is [26]:

$$V_{BE}(T) = \left[V_{G0} - \left(\frac{V_{G0} - V_{BE}(T_r)}{T_r} \right) T \right] + \left[(\eta - m) \frac{kT}{q} \ln \left(\frac{T}{T_r} \right) \right] \quad (3.3)$$

where V_{G0} is the silicon bandgap voltage extrapolated to 0 K (≈ 1170 mV), k is the Boltzmann constant, q is the charge of the electron, η is a parameter dependent of the fabrication process (typically $\eta \approx 3.5$), T_r is the reference temperature and $V_{BE}(T_r)$ is the transistor's base-to-emitter voltage at temperature T_r . The first terms of Eq. 3.3 is a CTAT voltage (Complementary To Absolute Temperature) that has a slope given by:

$$\frac{d}{dT} \left[V_{G0} - \left(\frac{V_{G0} - V_{BE}(T_r)}{T_r} \right) T \right] = \frac{-V_{G0} + V_{BE}(T_r)}{T_r} \quad (3.4)$$

which for typical values of $V_{BE} = 570$ mV measured at 300 K gives the well known result of -2 mV/ $^{\circ}$ C.

The second term of the $V_{BE}(T)$ expression, which presents a non-linear dependence with temperature, is very small when compared to V_{BE} , as shown in Fig. 3.5, where the MatLab plot of the difference between the values of V_{BE} calculated with and without the non-linear second term of of (Eq. 3.3) is presented. As it can be noticed in Fig. 3.5, the maximum value of this non-linearity error is $\pm 1.25 \mu\text{V}$ for a variation of temperature of ± 5 K around the room temperature 296 K. This is an error of 2 ppm when compared to V_{BE} normal values, and will be neglected.

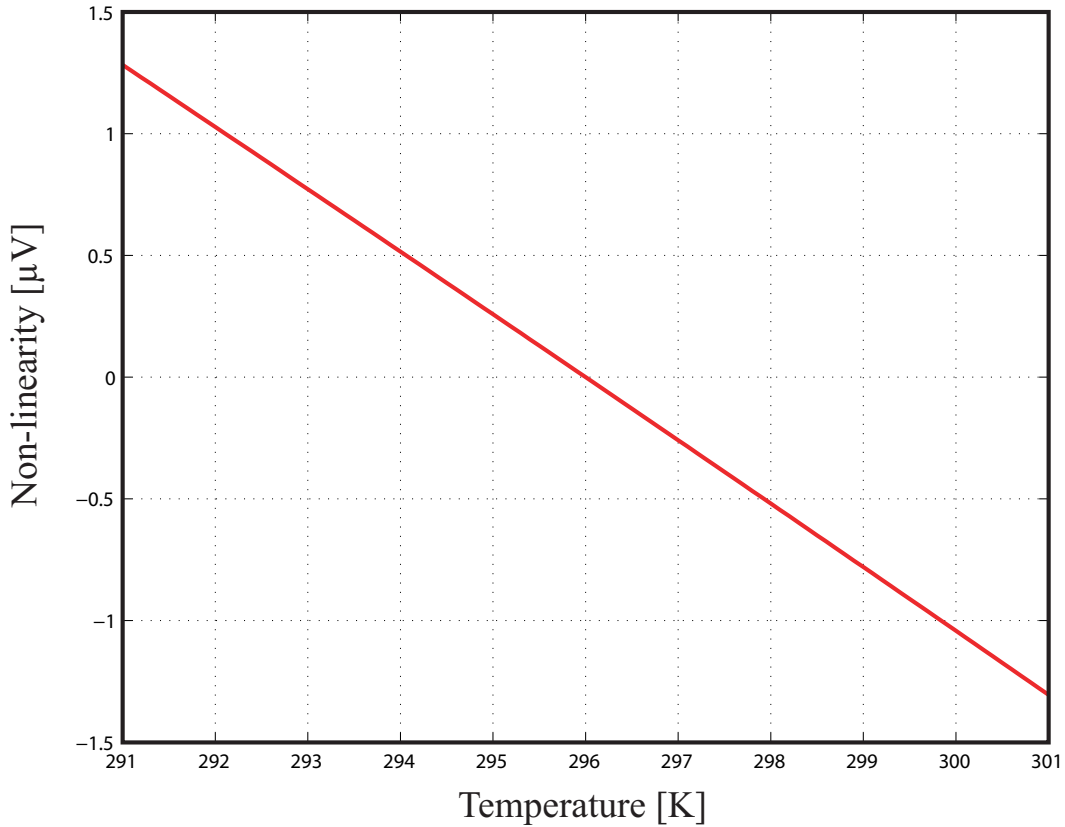


Fig. 3.5: Non-linearity of $V_{BE}(T)$ as a function the temperature.

Hence, if the V_{BE} of a transistor is measured at a given current I_{C_r} at a known temperature T_r , the thermal coefficient dV_{BE}/dT is calculated using Eq. 3.4, and then it is possible to obtain the temperature of the transistor simply by measuring the value of its V_{BE} .

This feature of the sensor is very important because a very simple calibration procedure can be employed in its fabrication. The sensors must be tested after fabrication to check if they are operating correctly and, in this proposed sensor, testing the sensor would be simply testing the transistor. If this test is performed in an environment with controlled temperature (or if the temperature of the room is measured), all that has to be done to calibrate the sensor is to measure the value of V_{BE} .

It is important to calculate the maximum error if no calibration procedure is done in the sensor. Since the variation in V_{BE} in the fabrication process of transistors is basically caused by variation of the base charge Q_B [27], this is the parameter which will be studied. For this calculation it will be assumed that a bipolar transistor can present a variation of 100% in Q_B due to process fabrication (this is an worst case conservative figure used by the manufacturers in the beginning of the 80s). Thus, two transistors Q_1, Q_2 with such a large difference in the base charge will have saturation currents given by $I_{S2} = 2I_{S1}$. When these transistors are biased with the same collector current $I_{C1} = I_{C2}$, one can write:

$$I_{C1} = I_{S1} e^{\frac{V_{BE1}}{V_T}} \quad (3.5)$$

and

$$I_{C2} = I_{S2} e^{\frac{V_{BE2}}{V_T}} \quad (3.6)$$

Dividing Eq. 3.5 by Eq. 3.6 and remembering that $I_{C1} = I_{C2}$ and $I_{S1} = 2I_{S2}$, it comes that:

$$V_{BE1} - V_{BE2} = \frac{kT}{q} \ln(2) \quad (3.7)$$

which is equal to $\approx 17.5\text{mV}$ at 300 K.

This result shows that the maximum variation of V_{BE} in all transistors from a manufacturer that controls the fabrication process to restrict the maximum variation of 100% in Q_B , the maximum variation found in V_{BE} for a given collector current will be $\Delta V_{BE} \approx 17.5\text{ mV}$ at room temperature. Using Eq. 3.4 to calculate the dispersion in dV_{BE}/dT caused by a 17.5 mV maximum error in V_{BE} , one concludes that the maximum deviation in dV_{BE}/dT will be $\pm 1.35\%$.

Hence, if errors in the order of 1.5% are tolerated by the application, uncalibrated sensors can be used. It is worth to notice that in modern microelectronics fabrication process, where critical steps like base doping are realized using ion implantation, Q_B presents a much smaller spread. For example, a substrate bipolar transistor fabricated in the TSMC CMOS 0.35 μm process present a maximum V_{BE} spreading of $\Delta V_{min} = -0.45\text{ mV}$ and $\Delta V_{max} = 0.40\text{ mV}$ [28]. For these transistors, the dispersion in dV_{BE}/dT would be reduced to $dV_{BE}/dT(min) = -1.9987\text{ mV}/^\circ\text{C}$ and $dV_{BE}/dT(max) = 2.0015\text{ mV}/^\circ\text{C}$, which represents an error of $\approx \pm 0.075\%$. If transistors with these tight controlled process parameters are used to fabricate the sensor, no calibration would be required.

3.4 A simple thermo-electric model of the complete sensor

In order to verify how the proposed SPHP will respond to the thermal and electrical stimulus, a simple thermo-electrical model for simulation of the sensors was developed. For the simulation of the electrical model, the transistor was driven by one pulsed current source and one pulsed voltage source, creating the same pulse of 150 mW ($I_C = 6$ mA and $V_{CB} = 25$ V) with duration of 10 s. To emulate the effect of the temperature in the V_{BE} of the transistor, the thermal model presented in Fig. 3.2 was added to the electrical schematic, as shown in Fig. 3.6.

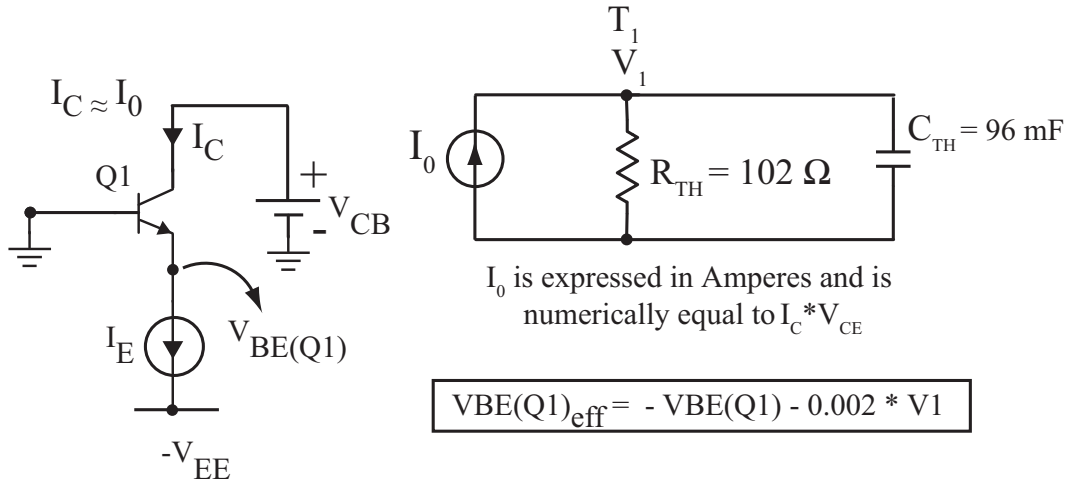


Fig. 3.6: Complete thermo-electrical model of the sensor.

The plotted values of $V_{BE_{eff}}$ are calculated by subtracting the variation $\Delta V_{BE}/\Delta T$ (assumed to be -2 mV/°C) from the constant temperature electrical simulation results of $V_{BE}(Q1)$. Therefore, the expression to calculate the plotted results of $V_{BE_{eff}}$ is:

$$V_{BE_{eff}}(Q1) = V_{BE}(Q1) - 0.002 \cdot T_1 \quad (3.8)$$

where T_1 is numerically equal to V_1 in Fig. 3.6.

The result from the simulation of the thermal-electric model is presented in Fig. 3.7, and it indicates that the proposed sensor shall work correctly, and that the measurement of the temperature can be easily performed, since values of ΔV_{BE} in the order of 9 mV must be obtained in the device for the agricultural range of θ_v .

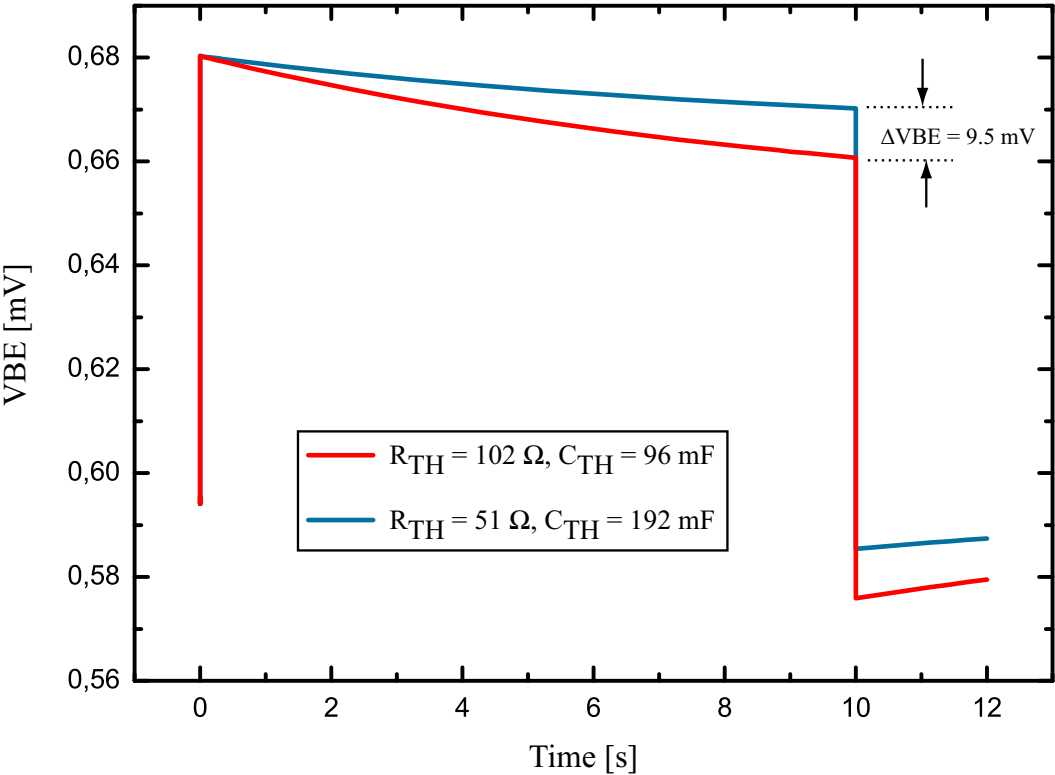


Fig. 3.7: Simulated results of $V_{BE}(t)$ for the same heat pulse applied, when two distinct heatsink materials are in contact with the sensor.

Chapter 4

Electronic Interrogation System

4.1 Principle of operation

THE interrogator of the sensor has to be an equipment that applies the heat pulse, measures the V_{BE} of the transistor (using an A/D converter), stores the data and finally transmits the measured data to a computer which will process the data and generate instructions for the irrigation system.

A block diagram of the complete interrogation system is shown in Fig. 4.1. Several power supplies voltages are necessary: a high power supply voltage to the circuits that create the voltage waveform of the heat pulse, a digital power supply for the microcontroller, an analog power supply for the microcontroller A/D converter and a split power supply to handle the analog circuits which will generate the current waveform of the heat pulse.

A microcontroller with an internal A/D converter is necessary to perform both digital control of the heat pulse and data transmission (via USB) to the computer, but also to make the A/D conversion of the V_{BE} values.

The transistor is driven by a current source connected to its emitter, so that the collector current $I_c = \alpha_F I_E$ (where α_F is the common base current gain) will be practically independent of the Early effect, and will also not depend strongly on the characteristics of the transistors, since a 100% variation in β_F from 400 to 200 causes a variation of only 0.25 % in α_F . Hence, if the current source I_E is well controlled, the power dissipated by the sensor will be well controlled and independent of the transistor's parameters.

Connecting the base of the transistor to ground is a very interesting choice because the voltages that need to be measured (V_{BE}) or applied (V_{CB}) in the circuit will be referenced to ground.

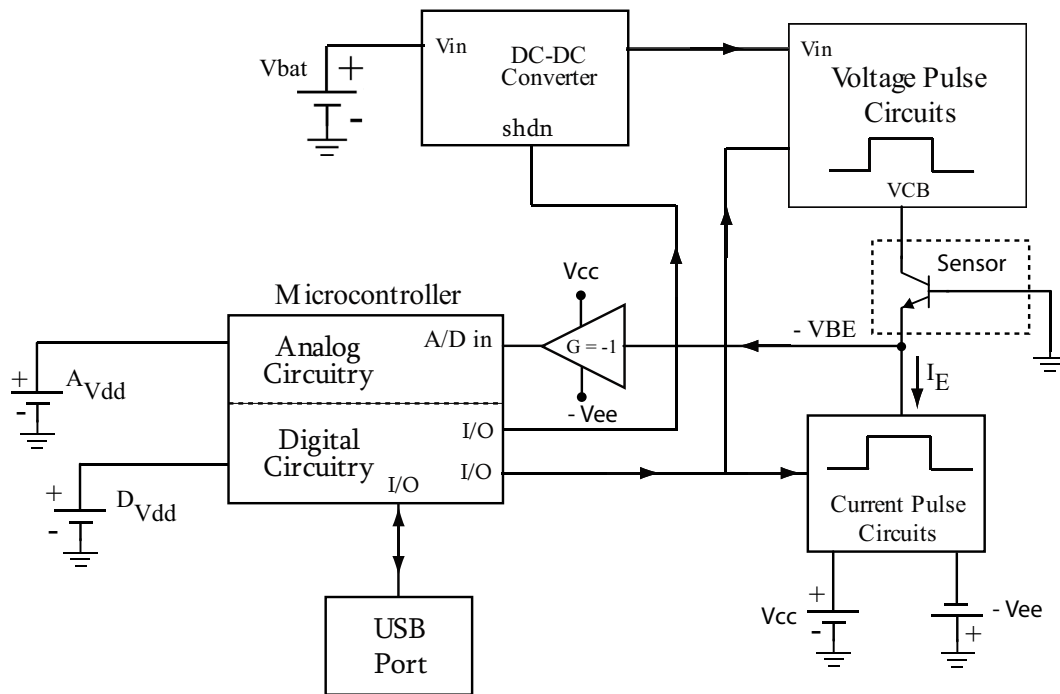


Fig. 4.1: Block diagram of the electronic interrogator

4.2 Voltage pulse circuit

To eliminate the risks of electrical shock and to allow the use of low-cost transistors, the voltage pulse that will be applied to create the heat pulse was chosen to be $V_{CB} = 25$ V. Since the interrogator has to be operated on batteries, it is necessary to use a dc-dc converter to generate this voltage. Since the heat pulse current will also be supplied by this circuit, it is important to choose rechargeable batteries which can last for many reading operations, to avoid interruption in the process of collecting data in the field.

From the simulations performed in Chapter 3, it was observed that a 150 mW heat pulse would be adequate to operate the sensor. If the voltage V_{CB} is equal to 25 V, the transistor current pulse will have to be 6 mA to reach the desired 150 mW power dissipation. Based on these data, the general conditions for the design of the dc-dc converter and the battery specifications are established. An operator working for 8 hours can read about 240 sensors, if it is assumed that the reading timing plus the dislocation time between sensors installed at a distance of 100 m is 2 minutes. Introducing a safety margin of 60 extra readings, it is desired that the interrogator can be able to read at least 300 sensors on a single battery charge, what leads to a minimum capacity of 5.0 mA.h for the battery.

This can be easily accomplished with very low-cost AAA Nickel-Metal-Hydride type batteries, since these cells have a nominal output voltage of 1.26 V per cell and 800 mA.h capacity, so the interrogator can operate a few months on a single battery charge. The other interrogator's circuits are low-power and will run at a much lower current level, so low-cost standard rechargeable Ni-Cd 9 V batteries cells will be used.

4.2.1 DC-DC converter

The first step in the interrogator project is, therefore, to design a dc-dc converter which will generate a power supply voltage adequate for the voltage pulse generator. A high-efficiency dc-dc converter that can operate with high voltages is the LTC1144 [29], which can operate with input voltages up to 18 V, presents a 93% efficiency, requires only 1.1 mA in active mode and has a power shutdown mode where the bias current is only $8\mu\text{A}$.

The simplified internal diagram of the LTC1144 along with external components D_1, D_2, C_A, C_B is presented in Fig. 4.2. The operation of this converter can be explained as follows:

The LTC1144 is a CMOS switched-capacitor voltage converter, with four internal switches. It has an internal oscillator that controls the switches with two clock phases, ϕ and $\bar{\phi}$. When the circuit is on the ϕ phase ($SW1$ closed and $SW2$ open) for the first time, C_A is not charged, since both the negative terminal of C_A and the anode of $D1$ are connected to V^+ ; C_B is charged through D_1, D_2 to a voltage equal to $V_{C_B} = V^+ - V_{D_1} - V_{D_2}$.

In clock phase $\bar{\phi}$ ($SW2$ closed and $SW1$ open), the negative pole of C_A is connected to ground, and the capacitor C_A charges through $D1$, to a voltage $V_{C_A} = V^+ - V_{D_1}$. The output capacitor C_B maintains its voltage $V_{C_B} = V^+ - V_{D_1} - V_{D_2}$.

When the circuit returns to clock phase ϕ , the negative terminal of C_A is once again connected to V^+ , however $D1$ does not allow the capacitor C_A to discharge, so it keeps its voltage of $V_{C_A} = V^+ - V_{D_1}$. With the negative terminal of C_A at V^+ , the output capacitor C_B charges through D_2 to a voltage $V_{C_B} = V^+ + (V^+ - V_{D_1}) - V_{D_2} = 2V^+ - V_{D_1} - V_{D_2}$. Hence, the output voltage of the dc-dc converter, present in capacitor C_B , will be equal to $V_{C_B} = V_{out} = 2V^+ - V_{D_1} - V_{D_2}$.

To reduce the voltage drop V_{D_1}, V_{D_2} , the Fairchild MBR735 Schottky diodes [30] (which have a forward voltage drop less than 380 mV at 1A) were used for D_1 and D_2 . A pack with 14 series AAA Nickel-Metal-Hydrate batteries was used, so $V^+ = 17.64\text{V}$ and $V_{out} \approx 34.5\text{ V}$ ($V^+ = 2 \cdot (17.64 - 0.38)\text{ V}$).

When the full agricultural range is considered, the simulations results presented in Chapter 2 shows that variations of ΔV_{BE} less than 5 mV are expected. Therefore, it is necessary to measure steps of $50\mu\text{V}$ to detect ΔV_{BE} variations with 1% resolution. To perform this measurement, the circuits must be low-noise circuits and a switching power supply like the dc-dc converter is certainly a source of noise. Since the current pulse lasts only 10 s, a simple solution was employed: the capacitor C_B was made large enough to allow for the shutting down of the dc-dc converter during the period of measurement.

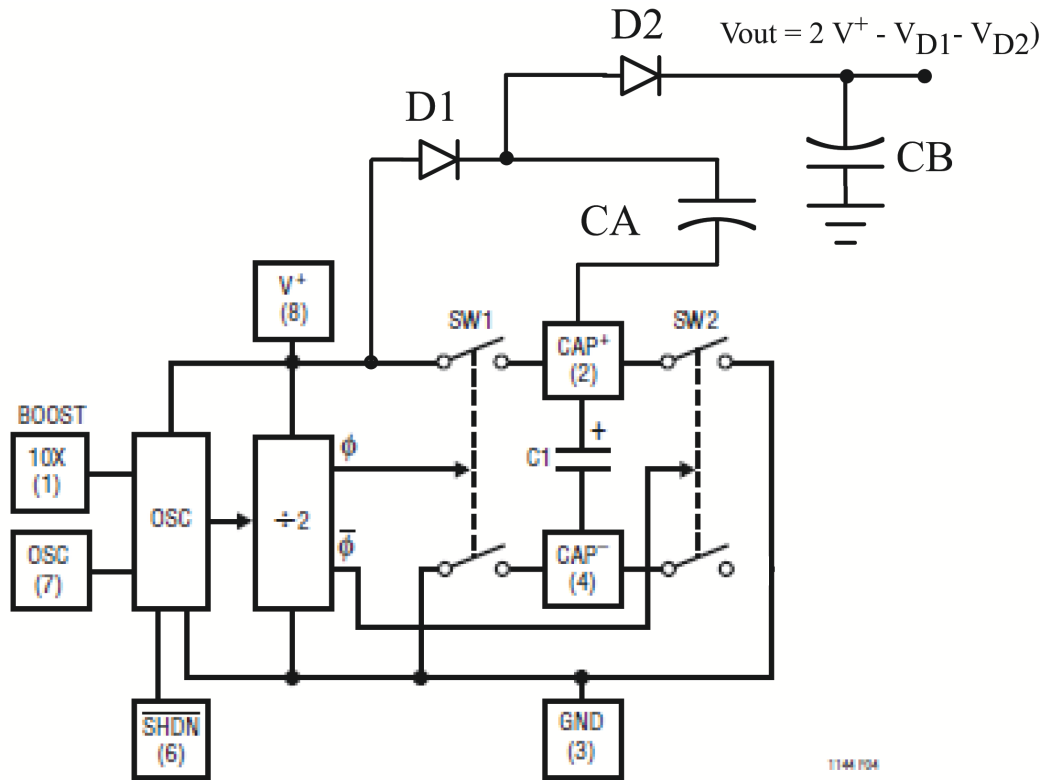


Fig. 4.2: Simplified internal block diagram of the LTC1144 switched-capacitor dc-dc converter

4.2.2 Voltage pulse generator circuit

The output voltage of the dc-dc converter depends on the battery voltage (V^+) and the voltage drops in the diodes V_{D1} , V_{D2} . So it cannot be used directly in the waveform generator of the voltage pulse, which requires a constant value ($V_{CB} = 25$ V). A voltage regulator combined with an op-amp and an analog switch were used to implement these functions, as shown in Fig. 4.3.

The voltage regulator LTC 3008 [31] has all features necessary to implement the voltage pulse generator: it operates with an ultra-low quiescent current ($3 \mu\text{A}$), accepts input voltages up to 45 V, has a low dropout (typically 270 mV @ 10 mA output current), and most importantly, it has an adjusting pin with a temperature stabilized voltage $V_{REF} = 600$ mV.

The output voltage of the regulator is given by:

$$V_{reg} = 600\text{mV} \left(1 + \frac{R_1}{R_2} \right) \quad (4.1)$$

The V_{CB} voltage (which is set at 0 V or 25 V) is delivered by the LT 1490, a low offset ($V_{OS} = 500 \mu\text{V}$) rail-to-rail micropower op-amp. The gain of the op-amp circuit, given by $G = (1 + R_3/R_4)$ is calculated to deliver 25 V when the 600 mV from the LTC3008's adjusting pin is present in its input. The required gain is $G = 41.667$, that is obtained using $R_3 = 453\text{k}\Omega$ and $R_4 = 11.1\text{k}\Omega$, both low thermal coefficient 1% metal film resistors.

The waveform pulse is generated by switching (with S_1) the non-inverting input of the op-amp

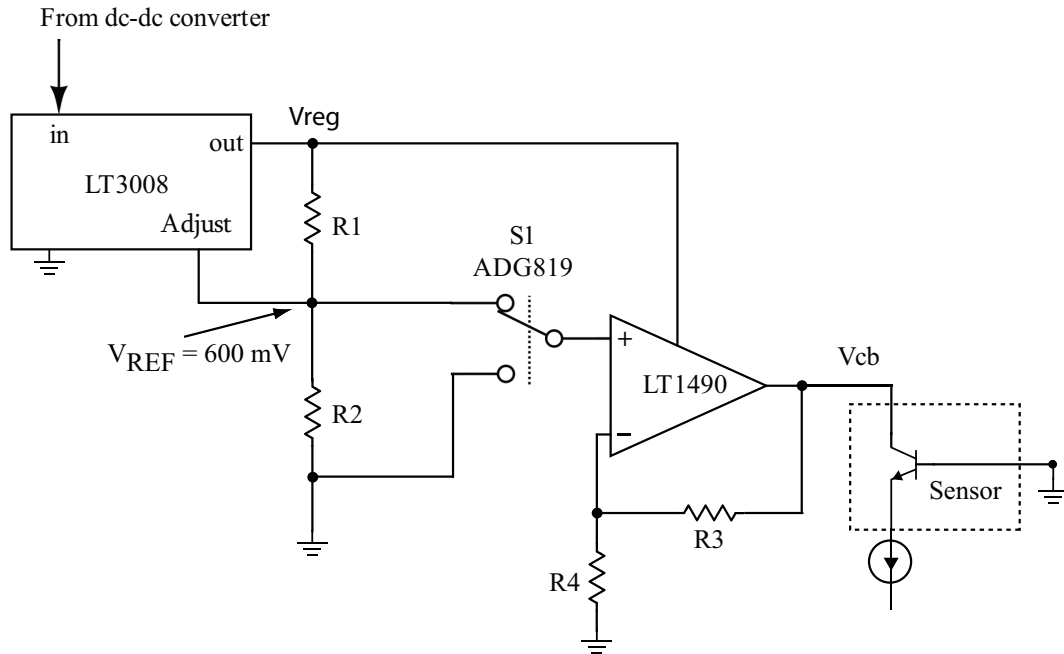


Fig. 4.3: Simplified schematic of the voltage pulse circuit

between 600 mV and 0 V. The power supply of the op-amp is the output voltage of the regulator, set at approximately 26.1 V, with R_1 , R_2 calculated by Eq. 4.1. Since the input current in pin *Adj* is very low (400 pA), high value resistors can be used for R_1 , R_2 in order to minimize the current drained by this voltage divider.

The minimum input voltage V_{in} for correct operation of the voltage regulator LTC 3008 has to be 270 mV above its output regulated voltage, or $V_{in} = (26.1 + 0.270) = 26.370$ V. Since the LTC 3008's input voltage is the output of the LTC 1144 dc-dc converter (which will be shutdown during the application of the heat pulse), it is necessary to use a capacitor C_B that will present a maximum voltage drop of $\Delta V = 34.5 - 26.37 = 8.15$ V after a $\Delta t = 10$ s pulse with a current $I = 6$ mA. The value of C_B is calculated from:

$$C_B = I \frac{\Delta t}{\Delta V} = 6 \text{ mA} \frac{10 \text{ s}}{8.15 \text{ V}} = 7360 \mu\text{F} \quad (4.2)$$

It is interesting to notice that V_{reg} and V_{CB} are both dependent on resistor ratios (R_3/R_4 , R_1/R_2), which are very stable with temperature and tied to a single reference voltage V_{REF} , so despite of variations in the value of V_{REF} (maximum of 1% according to the data-sheet) the circuit will always operate correctly.

The measured result from the dc-dc converter circuit (powered with a $V^+ = 15.5$ V power supply) and the voltage regulator circuit are presented in Fig. 4.4 (a) and (b).

Since the voltage regulator is a low dropout type (270 mV), its output stabilizes at the desired $V_{reg} = 25$ V immediately after the dc-dc converter passes the 25 V voltage level, what occurs approximately 940 ms after the circuit is turned on. However, the capacitor C_B in the dc-dc converter is not yet fully charged at this time, and it is necessary to wait about 2.5 s (due to the switched-capacitor action) before the output of the dc-dc converter stabilizes at 30.4 V and a measurement of the sensor

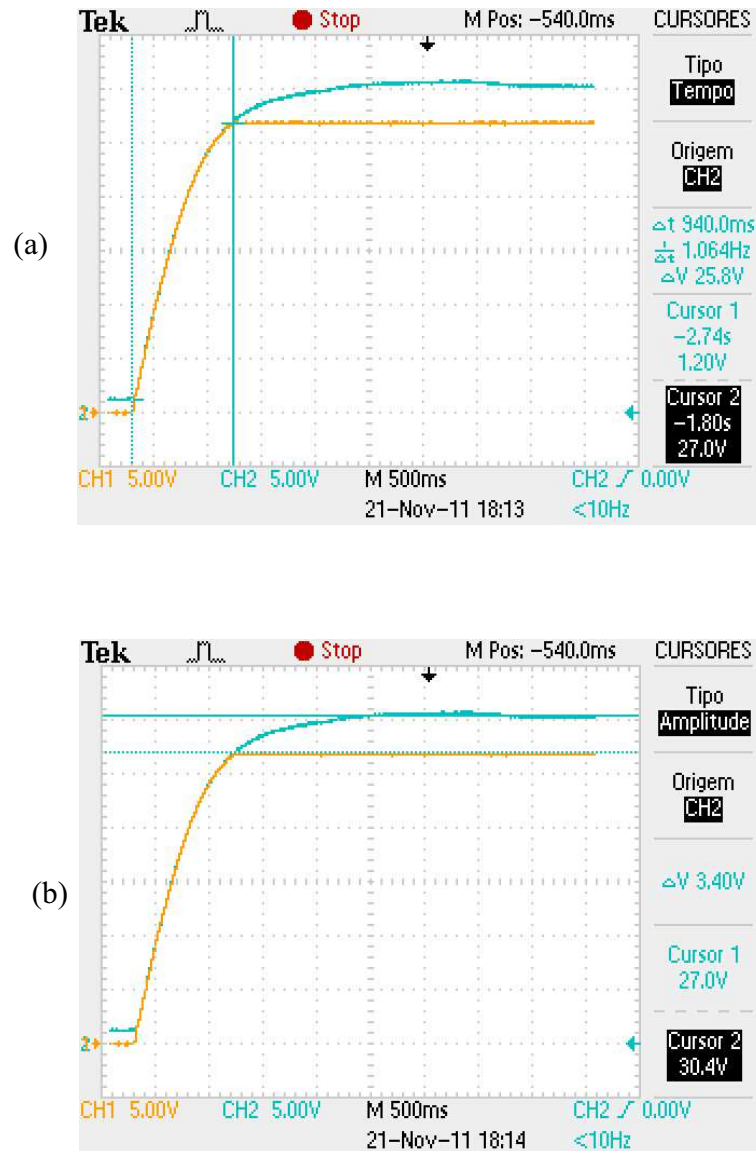


Fig. 4.4: Measured result in the output of the dc-dc converter and voltage regulator.

can be taken.

The measured result in the output of the op-amp (voltage pulse) is presented in Fig. 4.5. The amplitude of the pulse presents the desired value, from 0 to 25.0 V.

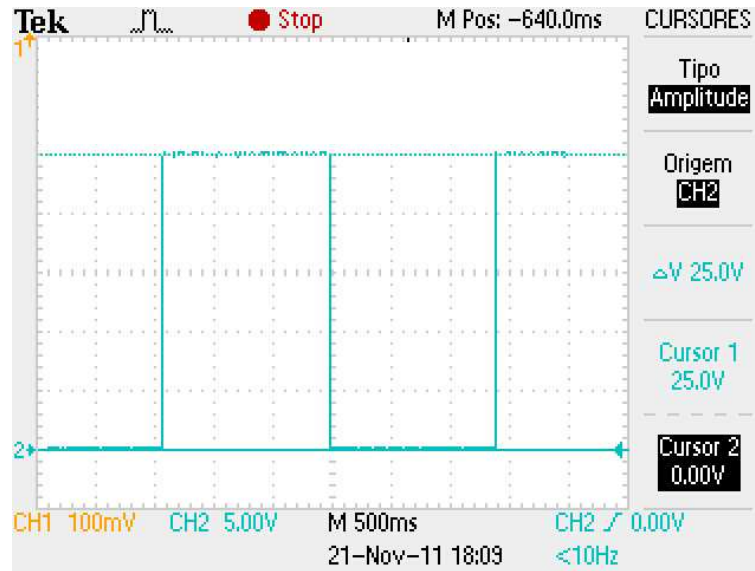


Fig. 4.5: Measured result of the voltage pulse in the output of the op-amp.

4.3 Current pulse generator circuit

The basic idea to produce the current pulse is through the switching of two different current sources, as shown in the block diagram presented in Fig. 4.6.

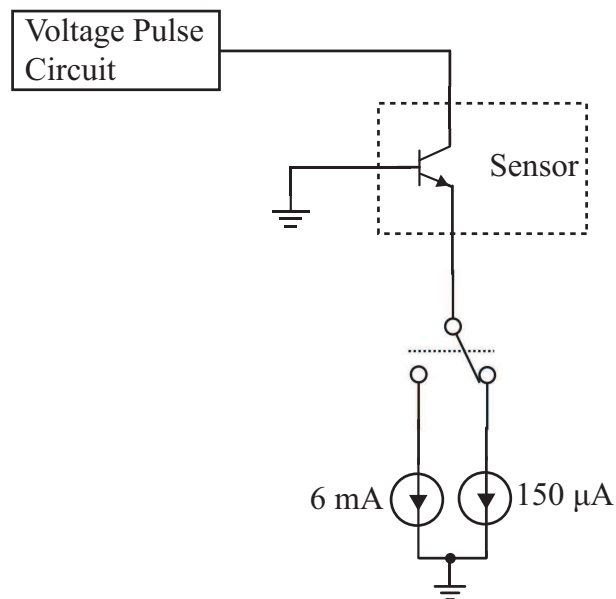


Fig. 4.6: Block diagram of the current pulse generator circuit

The current pulse amplitude will vary from a low current $I_{ci} = 150\mu\text{A}$ (that will not self-heat the sensor when $V_{CB} = 0$) to a heat current of $I_{cm} = 6\text{mA}$. The current waveform generator circuit developed uses an op-amp, a current source, a current mirror and an analog switch. The simplified

schematic of the developed circuit is shown in Fig 4.7.

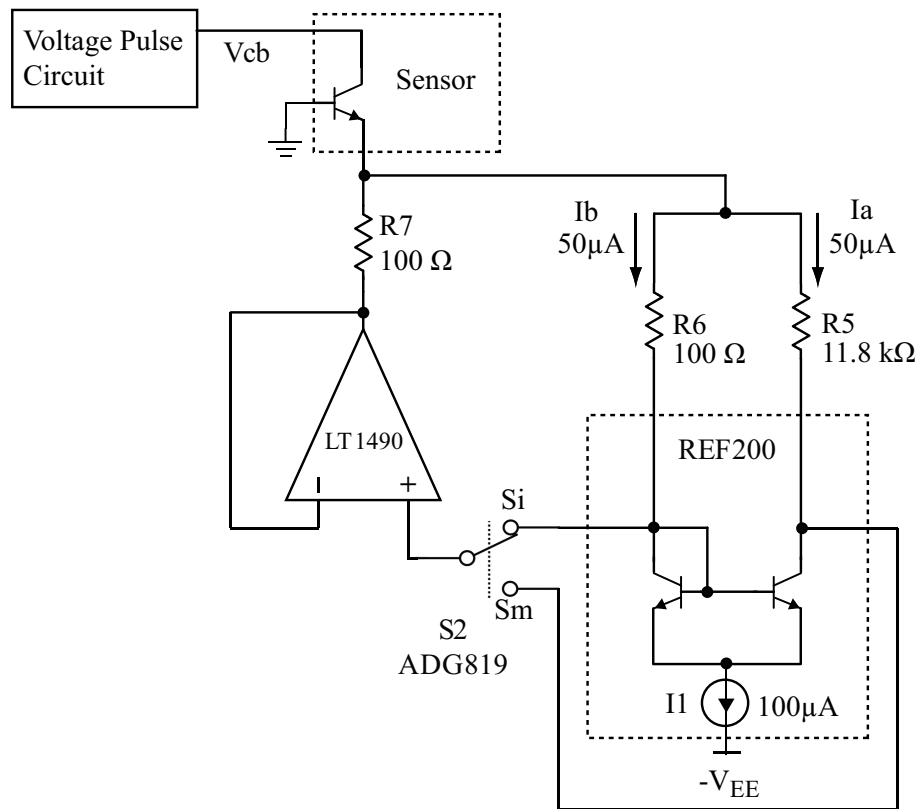


Fig. 4.7: Block diagram of the current pulse generator circuit

The REF200 IC has two $100\mu\text{A}$ precision current sources and one current mirror. In the developed circuit the current mirror is used to divide one of the $100\mu\text{A}$ current sources (I_1), in order to produce two identical $50\mu\text{A}$ current sources (I_A and I_B). The second current source in the REF200 (I_2) is not used and do not drain any current if its output pin is left open.

Current sources I_A and I_B are connected to the transistor's emitter through resistors R_5 and R_6 , forcing the transistor to deliver $100\mu\text{A}$ to those resistors. The transistor also supplies the current drained by the op-amp output (through resistor R_7). When the switch S_2 is in position S_i , the voltage drop in resistor R_7 is the same as in R_6 . Therefore, by making $R_7 = R_6$, the current through R_7 will be $50\mu\text{A}$, and the total current sinked from the transistor is $150\mu\text{A}$.

When the switch is changed to position S_m , the voltage drop in resistor R_7 is the same voltage drop around R_5 . Therefore, by making $R_5 = 118R_6 = 11.8\text{ k}\Omega$, the current through R_7 will be $I_{R7} = 188 \cdot 50\mu\text{A} = 5.9\text{ mA}$, and the total current sinked from the transistor is 6 mA as desired.

The measured result from the current pulse circuit is presented in Fig. 4.8. A value of 6.32 mA was obtained because the value of R_5 in the circuit was a little higher, $12.7\text{ k}\Omega$.

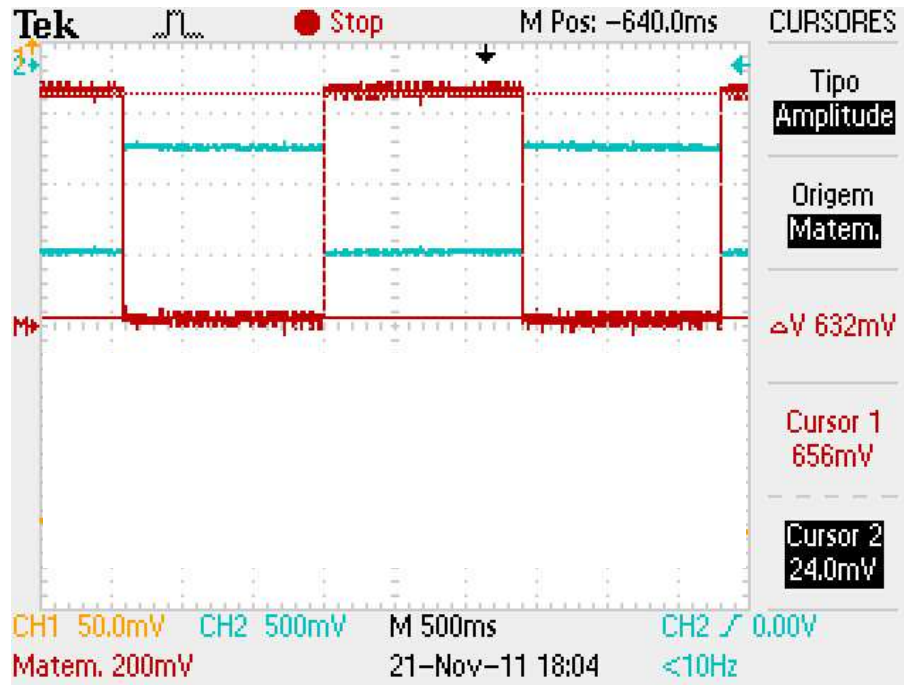


Fig. 4.8: Measured result of the current pulse generator circuit

4.3.1 Analog switches

As it has been previously presented, the circuits developed to generate the heat pulse (voltage and current) require two analog switches. In both circuits the analog switch is connected to the input of an op-amp, so there is practically no current flow through the switches. The analog switch in the voltage circuit (S_1) operates with input voltages of 0 V and 600 mV. The other switch (S_2) has input voltages of $(-V_{BE}(Q1) - V_{R6})$ and $(-V_{BE}(Q1) - V_{R7})$, which are approximately -570 mV and -1.2 V.

To reduce the circuitry, it is interesting to use the same clock signal and the same power supply for both analog switches. The analog switch ADG819 from Analog Devices [32] can operate with a 5.5 V power supply and accepts rail-to-rail input voltages,. Thus, if S_1 and S_2 are powered by a ± 2.5 V supply, the minimum and maximum input voltages (600 mV from S_1 and -1.2 V from S_2) will fall within the specified operational range.

The only problem left to be solved is in what concerns the clock signal, which will be taken from the output of a microcontroller and has an amplitude of 0 V (digital “0”) and 3.3 V (digital “1”). For the ADG819, the V_{iH} (minimum voltage interpreted as a digital “1”) is 2 V, and the V_{iL} (maximum voltage interpreted as a digital “0”) is 0.8 V when relative to the ground reference. Since in this design the analog switches are referenced to -2.5 V, it is easy to calculate that the clock signal has to be lower than -1.7 V and higher than -0.5 V to be recognized as a digital “0” and a digital “1”, respectively.

A simple but effective solution was employed, using an op-amp in the inverter configuration, with a gain $R_8/R_9 = 0.667$. When the input voltage is zero, the output voltage will be zero, which meets the requirement of being ≥ -0.5 V to be taken as a digital “1”. When the input voltage is 3.3 V, the op-amp’s output voltage will be approximately -2.2 V, which meets the requirement of being ≤ -1.7

V to be taken as a digital “0”.

The schematic of the power supplies and the conditioning of the clock for the analog switches is shown in Fig. 4.9. The ± 2.5 V supply voltages are derived from two LT1004 low-cost two-terminal voltage reference ICs [33] and the ± 9 V sources shown were implemented by standard 9 V rechargeable Ni-Cd batteries, as mentioned earlier.

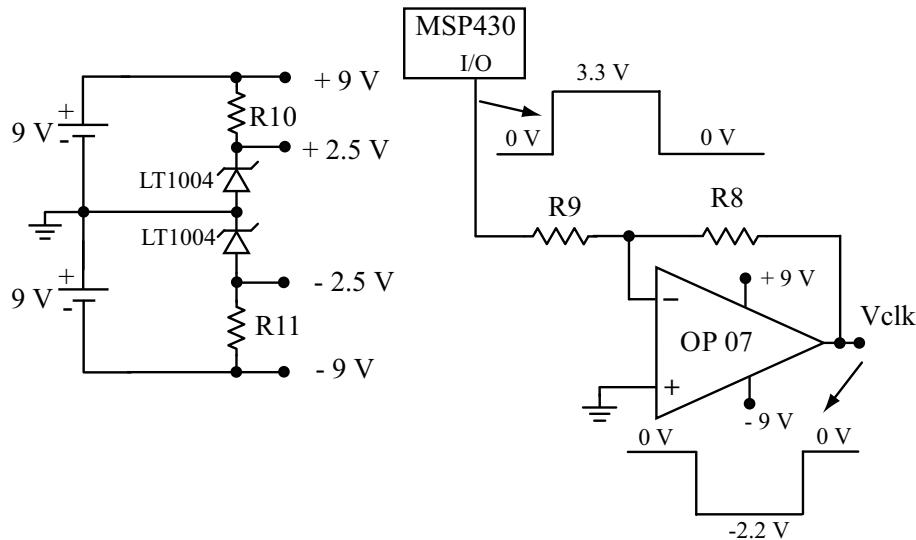


Fig. 4.9: Schematic diagram of clock conditioning circuit for the analog switches and ± 9 V and ± 2.5 V power supplies

The measured result of the clock signal in the output of the inverter amplifier op-amp is presented in Fig. 4.10. Values of 0 V and -2.25 V were observed.



Fig. 4.10: Measured result in the output of the op-amp (clock signal of the ADG819 switches).

4.3.2 The microcontroller and the USB communication circuit

As it was previously mentioned, the interrogation circuit developed uses a microcontroller which is responsible for controlling the analog switches S_1, S_2 , making the V_{BE} measurements (with an internal A/D converter) and transmitting the stored measured data to a computer. The MSP430AFE251 microcontroller was used on the project, since it is ultra low-power IC, has a 24 bits A/D converter, and can transmit data via a SPI interface, which is very useful to communicate with USB data converters.

The full scale value of the internal A/D converter of the MSP430AFE251 is set internally to 1200 mV, so it should be possible to make the measurements of V_{BE} directly. However, in the measurement scheme used, the values of V_{BE} are negative (the base of the transistor is connected to ground), so an op-amp is required to invert this signal, as shown in Fig. 4.11, where the complete schematic of the microcontroller and USB communication circuits is presented. Although the A/D converter can operate with 24 bits, in this application it is being used with 16 bits, what results in a resolution of $18.3\mu\text{V}$. As it is expected that variations of V_{BE} in the order of millivolts will be measured, the resolution provided by the 16 bits A/D converter must be sufficient to make the tests and validate the concept of the new sensor.

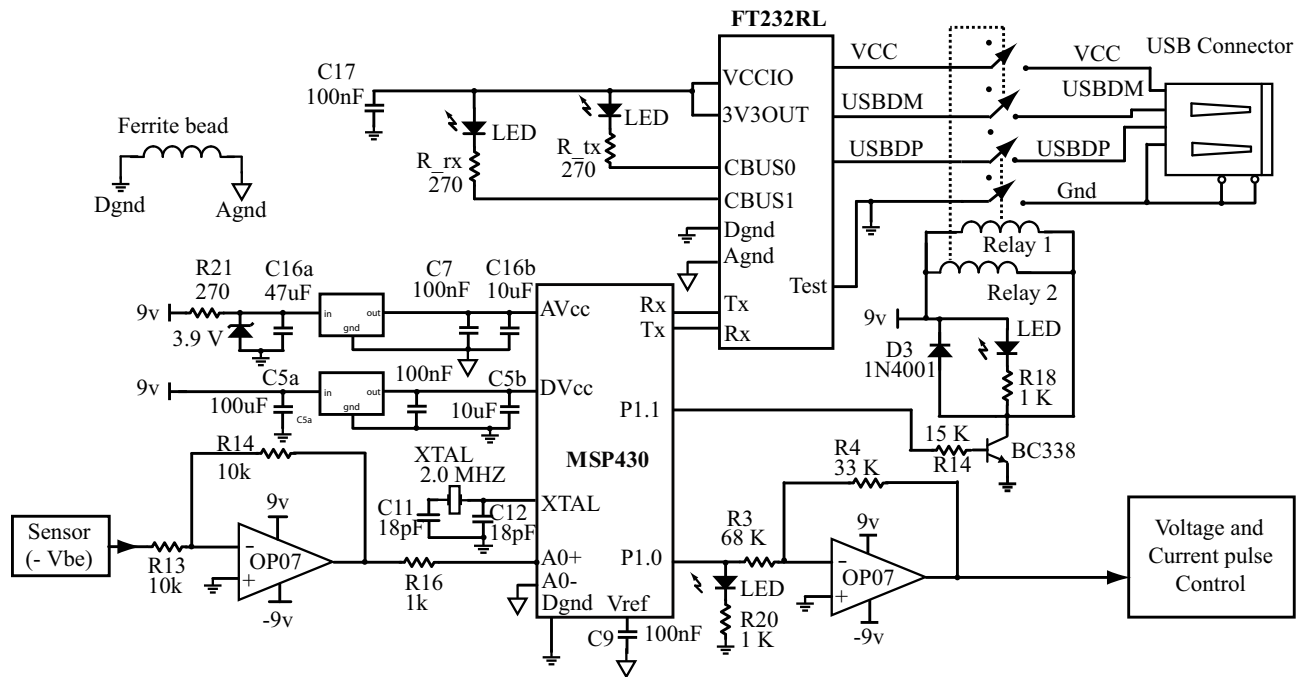


Fig. 4.11: Schematic diagram of the microcontroller and USB circuits

The MSP430 has two separated $V_{DD} = 3.3\text{ V}$ sources, one for the digital part and the other for the analog circuits. In most applications the analog AV_{dd} can simply be derived from the DV_{dd} using a low-pass filter. However, when it is desirable to reduce the noise in the analog part as much as possible, the use of two separate sources is highly recommended. Another recommendation to reduce the noise in the analog part is to create two separated grounds, $AGND$ and $DGND$, which are connected by a ferrite bead, avoiding the noise from the high speed switching digital part to reach

the analog ground.

As per the specification of the MSP430 data-sheet, the power must be supplied first (or exactly at the same time) to the digital DV_{dd} and then to the AV_{dd} . Since two separated voltage regulators were used, and it is not possible to guarantee which one would ramp-up its output voltage before the other, an external filter was inserted to introduce a delay in the AV_{dd} signal .

To implement the USB serial communication, a USB-UART converter (FT232RL) was used [34]. This IC receives the data from the SPI Rx/Tx ports of the microcontroller and converts the data to be used directly in USB port. The interrogator, when in regular use in the field, would store the sensors measured data and the transmission of this data to the computer (via the USB port) would be done only at the end of the measurements (typically a day of work). Thus, all analog measurement would not be disturbed by the noise generated by the connection of the grounds of the computer and the interrogator, via the USB port.

Since this prototype was designed to be used in laboratory, where after each measurement the data would be transferred to the computer to be studied, and it was not practical to connect/disconnect the USB cable for every measurement, a simple solution was adopted, by connecting the USB socket to the pins of the FT232RL through a relay, which is controlled by the MSP430 microcontroller. Thus, the USB cable is permanently plugged in the prototype but their pins are connected to the circuit (by the microcontroller and the relays) only when a V_{BE} measurement is finished. Consequently the system runs at very low noise during the measurement phase, since all the major sources of noise are well isolated: the USB is disconnected, the dc-dc converter is shut-down, the AV_{dd} is separated from the DV_{dd} , and the $AGND$ is isolated from the $DGND$ with a ferrite bead.

This effort to isolate the noise sources proved to be very successful, as can be noticed in Fig. 4.12, where a constant voltage was measured.

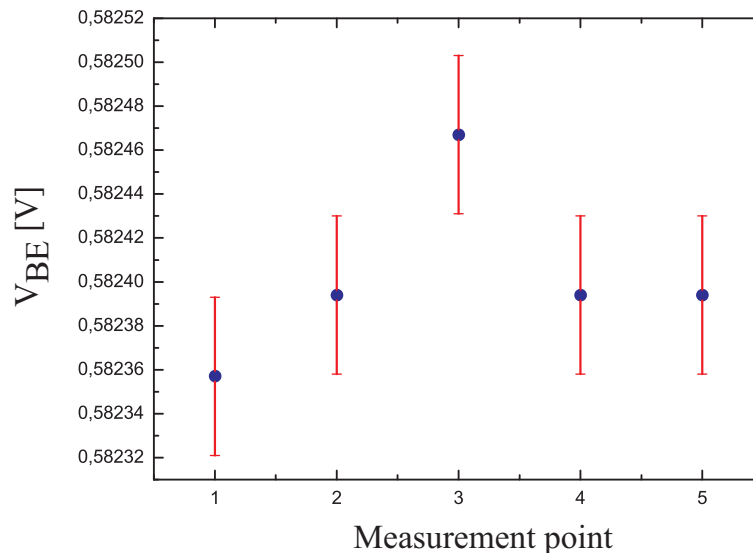


Fig. 4.12: Measurement of a constant V_{BE} voltage, showing that a low-noise circuit was achieved

The plot shows five consecutive measurements taken with the interrogator from a V_{BE} of a 2N2222 transistor, where the red bars indicate the error of ± 1 LSB ($\pm 18.3\mu\text{V}$) inherent to the A/D converter. It is important to notice that this measurement was taken without any type of shielding (the

circuit board was open, over the bench) and MINIPA MPL3303 power supplies (connected to the 127 AC line voltage) were used. If the interrogator had been shielded inside a metallic box and powered with batteries, it is likely that an even better result could possibly be obtained.

The complete schematic of the interrogator is presented in Fig. 4.13 and the layout, routed in a double-layer PCB board, is shown in Fig. 4.14.

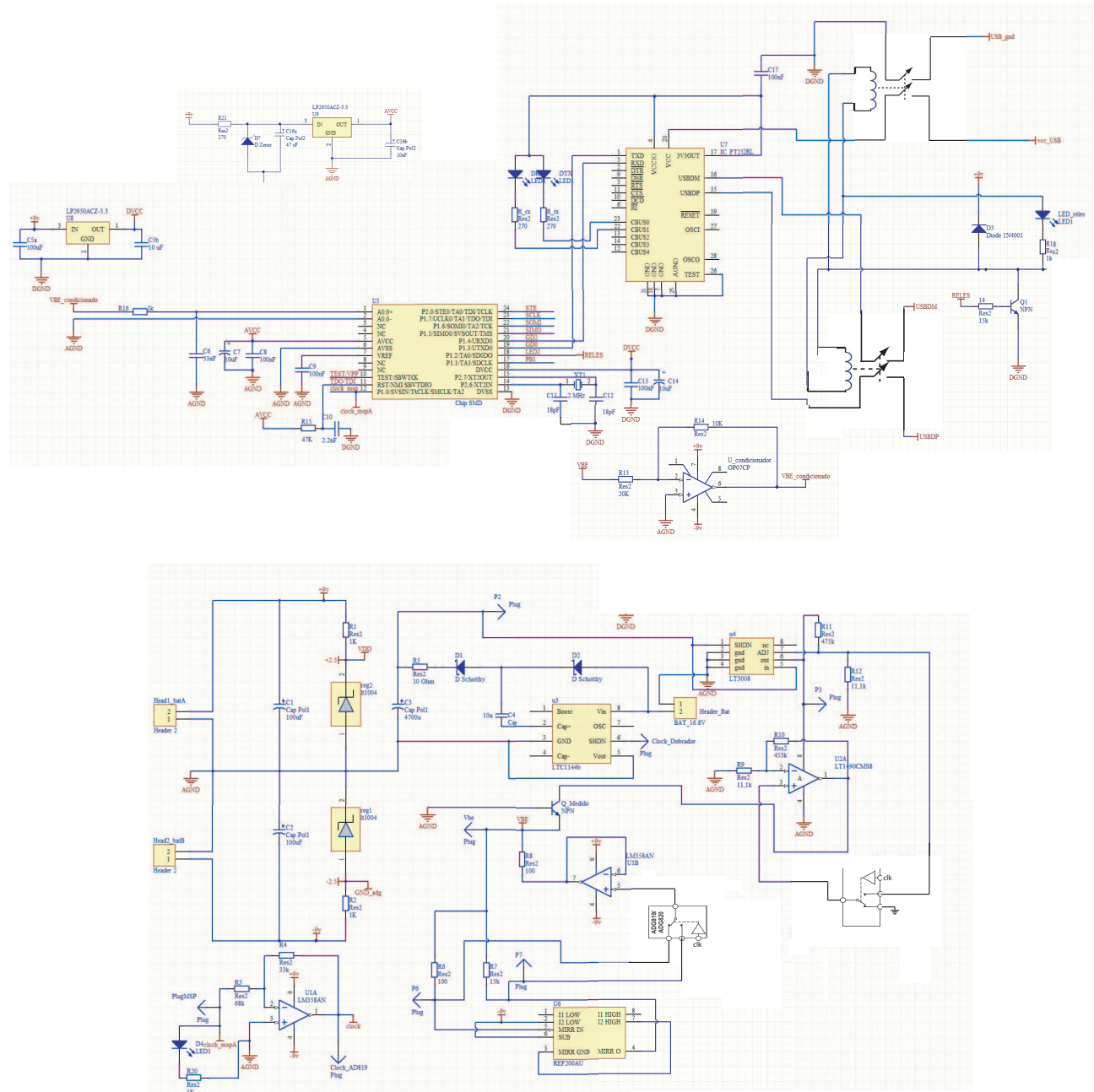


Fig. 4.13: Complete schematic of the developed interrogator

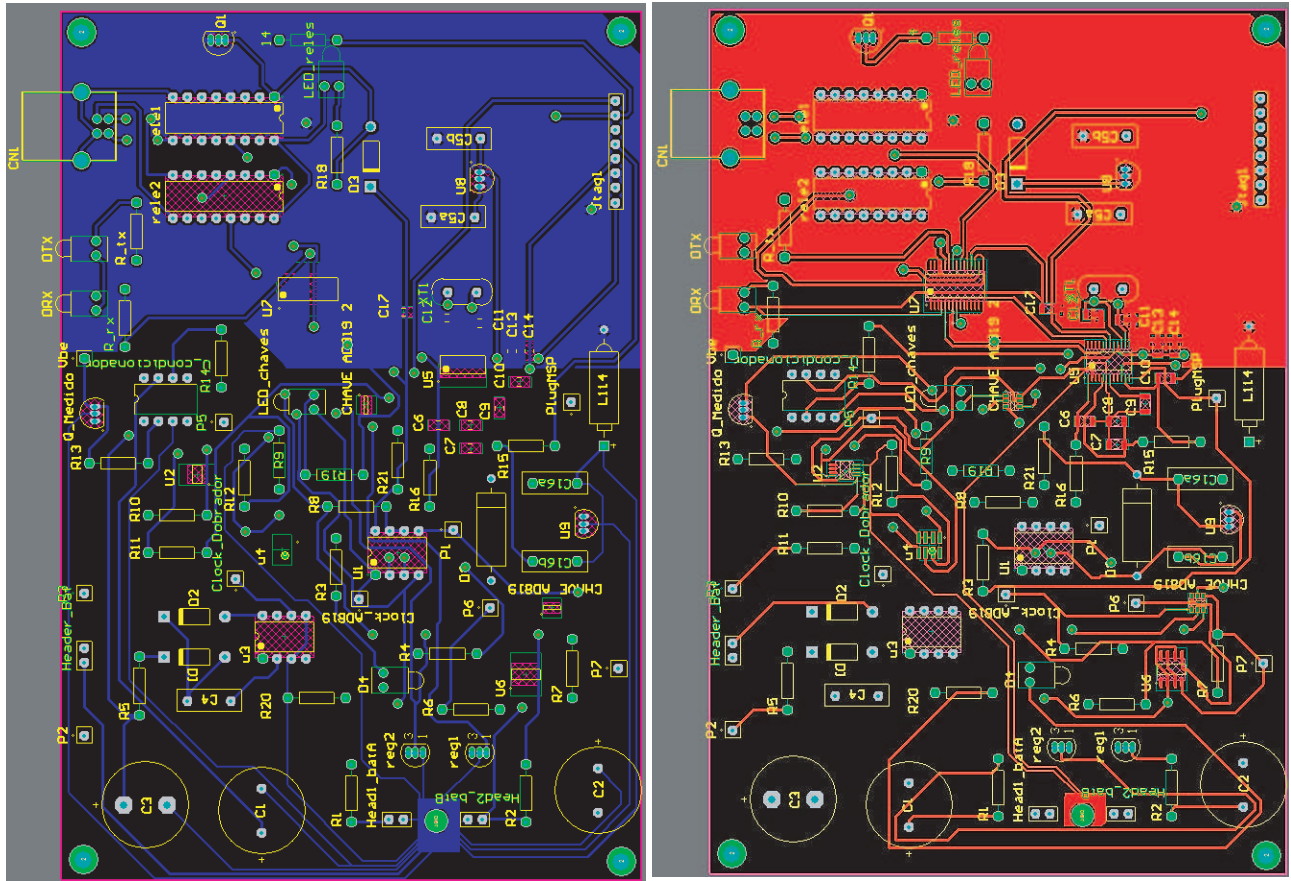


Fig. 4.14: Layout of the double-layer PCB designed for the interrogator

Chapter 5

Characterization of the sensor

5.1 Basic functional tests

TO make the humidity tests, several sensors were prepared using metal can transistors (2N2222) and plastic transistors (BC547). The transistors had wires soldered to their lead terminals and a silicone film was applied over these connections to electrically insulate these conductors. Some of the sensors were encased in a gypsum block, in order to test the proposed technique using the traditional porous block configuration.

The interrogator was programmed to apply the heat pulse ($I_C = 6 \text{ mA}$, $V_{CB} = 25 \text{ V}$) for a period $t_m - t_i = 10 \text{ s}$. In order to obtain data from all phases of the measurement, the A/D converter was programmed to measure the V_{BE} as follows: 5 points are measured before the heat pulse, 185 points are measured during the 10 s heat pulse and, finally, 9 points are measured after the end of the heat pulse.

A LabView Program was written to open the USB communication serial port of the computer, connect to the FT232RL and receive the measured data stored in the MSP430 microcontroller. In this work, since the objective was to test the technique and the new sensor, the measured data was stored in the RAM of the MSP430. In an interrogator designed to read hundreds of sensors in the field, it would be necessary to add a mass memory to it and probably the best solution would be the use of a flash memory. A print of the LabView screen with the plotted results of a V_{BE} measurement of a plastic BC547 transistor (in air) is presented in Fig. 5.1, where it is observed the acquired points during the three phases of measurement.

To test the operation of the interrogator and obtain basic comparative data about the sensor, a device made with a 2N2222 transistor was measured both in the open air and inserted into a soil. In Fig. 5.2 it is shown the measured results of the V_{BE} of the sensor, where it can be observed that a variation of V_{BE} in the order of 3 mV is obtained just before the end of the 10 s heat pulse.

In order to plot the three phases in the same graphic, these two plots have different time scales ($x - axis$). During the heat pulse the time between each measured point is 54 ms, and there are 185 measured points (points No.6 to No.190). In the other phases (before and after the heat pulse), the time between each measured point is only 6.17 ms. Six points (points No.0 to No.5) were measured before the heat pulse, and 9 points (No.191 to No. 199) were acquired after the end of the heat pulse). Thus, to avoid making a plot with three scales in the time axis, all graphs which have these different time scales will be plotted with the $x - axis$ given by the point position.

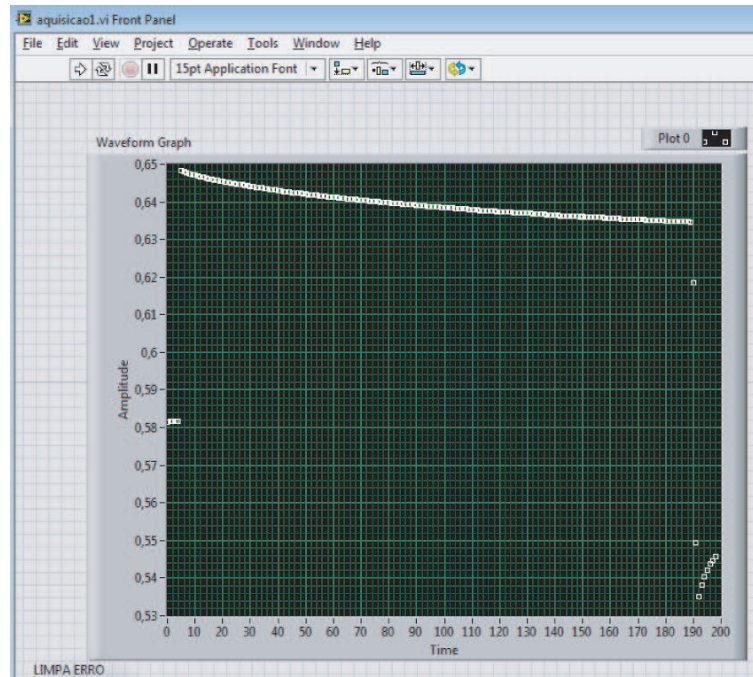


Fig. 5.1: Labview plot of the measured V_{BE} , showing the three phases of measurement.

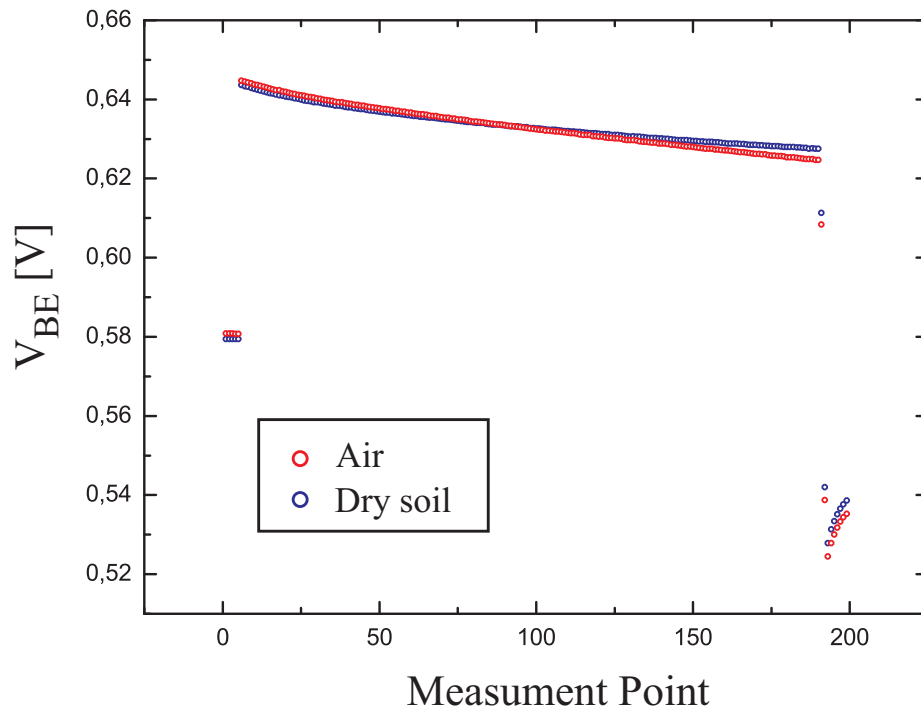


Fig. 5.2: Plot of the measured V_{BE} of a sensor prepared with a 2N2222 transistor in air and inserted in a dry soil.

Examining the lower portion of the measured V_{BE} curve in Fig. 5.3, just after the heat pulse was removed from the sensor, one notices that there is a quick change in temperature because the sensor cools quickly, transferring heat to the heatsink (soil or air).

As the A/D converter was set to read data at a sampling rate of 162 samples/s, the time between two consecutive measurements after the heat pulse is removed is about 6.17 ms. Thus, a variation of 1.5 mV in V_{BE} is found in only 55 ms, and picking up a single value in this region can lead to measurement errors. This part of the curve will be analyzed in detail in next sections to derive a method for using this region to measure the $V_{BE}(T)$.

When calculating the V_{BE} data to convert the measured points to ΔT , the resulting plot (presented in Fig. 5.3) showed a very interesting and intriguing fact. The temperature of the sensor *increases* substantially when the heat pulse is removed.

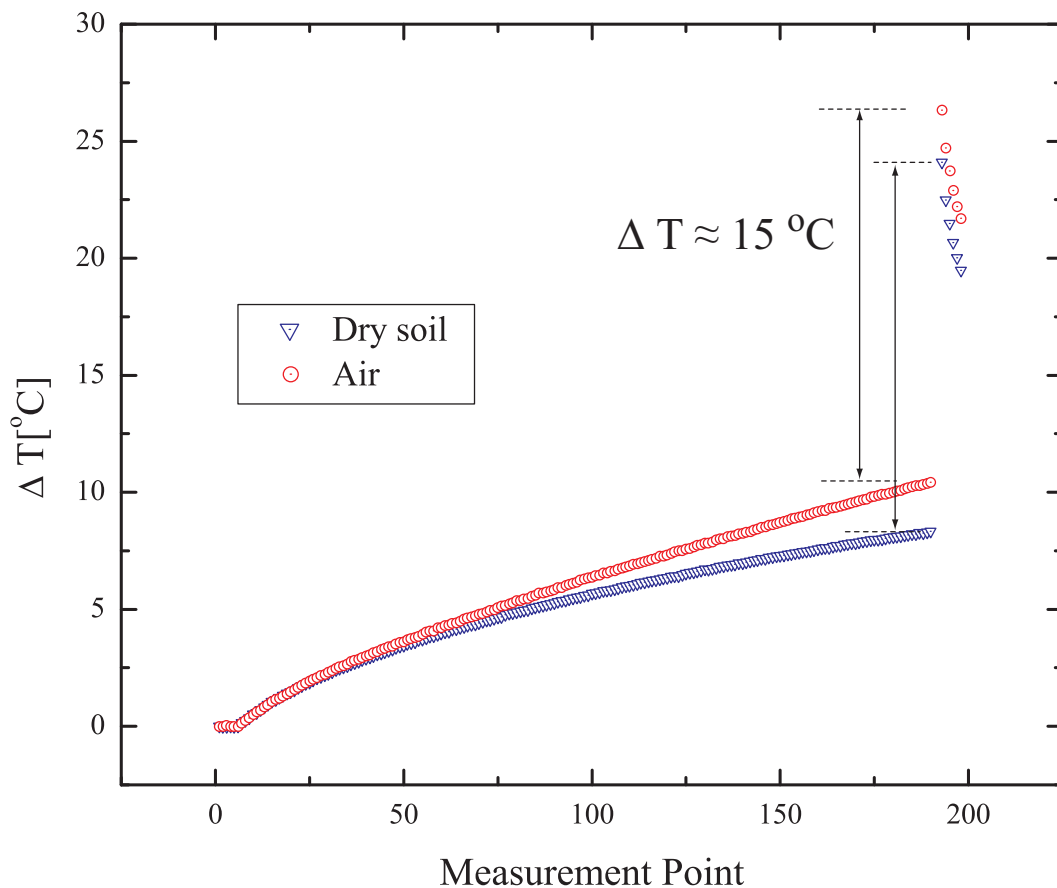


Fig. 5.3: Plot of the calculated temperature in the sensor, from $V_{BE}(T)$ measurements presented in Fig. 5.2.

It becomes clear that there is something wrong with the temperature calculated values, since there is no reasonable physical interpretation for such behavior. How would it be possible to the temperature of the transistor increase by a large amount, almost instantaneously after the heat pulse is removed. Since there is no doubt about the measured values of V_{BE} , the only explanation for this strange temperature calculated values is that there is a very fast, almost instantaneous heating of the transistor at the beginning of the measurement phase, immediately after the heat pulse is applied.

If this hypothesis is true, the first point of V_{BE} measured (6.17 ms after the heat pulse is applied) is the V_{BE} of a transistor that has been already considerably heated. So, since the reference to calculate ΔV_{BE} (and consequently ΔT) during the heat pulse is exactly this first value of V_{BE} , to reflect the actual values of temperature in the transistor's junction, the whole curve of $V_{BE}(T)$ during the heat pulse has to be level-shifted by this quasi-instantaneous temperature increase.

If one compares the last measured temperature point during the heat pulse with the first point after the heat pulse is removed, it is reasonable to admit that these temperatures are equal (or at least very close). So, in order to make these temperatures equal (or very close) in the graph of Fig. 5.3, the correct curve of the temperature during the heat pulse must be level-shifted by 15°C . A plot of the curve after applying the proposed correction (level-shifted by 15°C) is presented in Fig. 5.4.

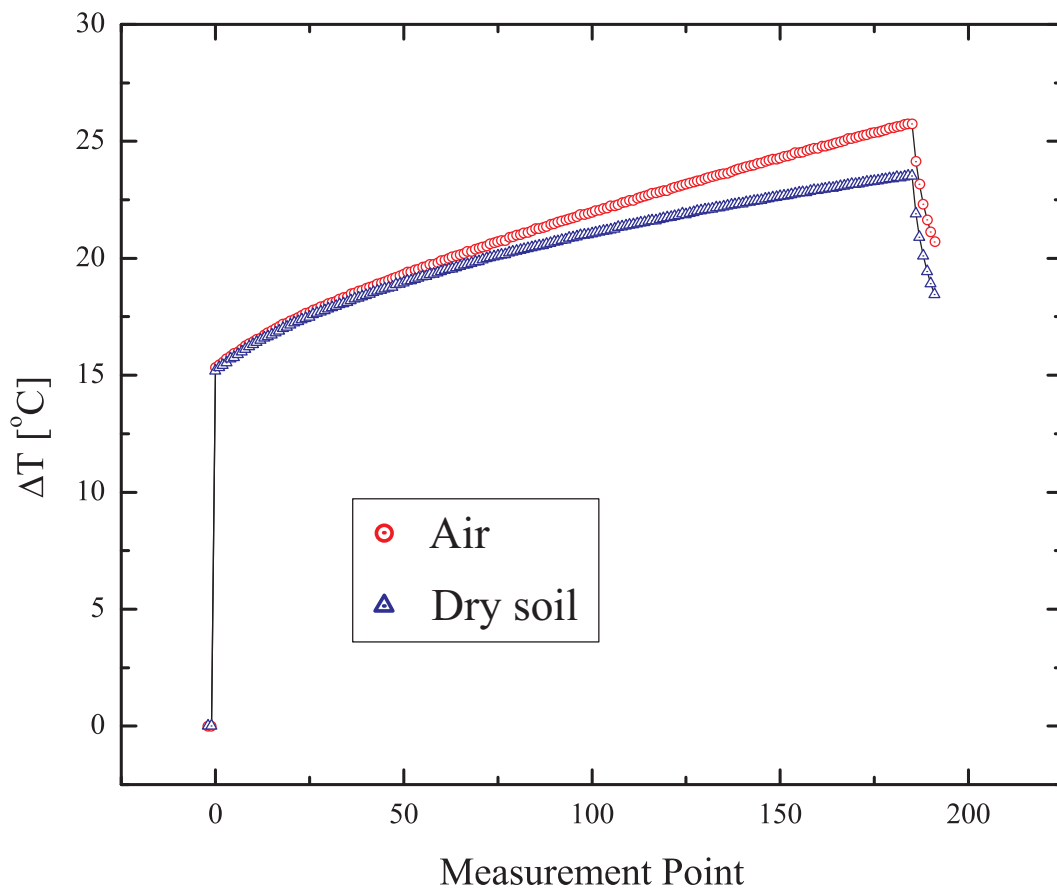


Fig. 5.4: Plot of the calculate temperature in the sensor, from $V_{BE}(T)$ measurements, after proposed temperature correction.

It is possible to verify if this theory is correct by calculating the V_{BE} of the transistor using its electrical model. For a transistor maintained at a constant temperature T_0 , if a current pulse from $IC_1 = 150\mu\text{A}$ to $IC_2 = 6.32\text{mA}$ is applied, a variation of $\Delta V_{BE} = V_T \ln(6.32\text{mA}/150\mu\text{A}) = 96.14$ mV is expected to be measured. From the measurement of V_{BE} taken 6.17 ms after the heat pulse is applied, it is observed that a variation of only 64 mV was measured (63.98 mV for the transistor left in the air and 64.16 mV for the transistor inserted into a dry the soil).

The first explanation to this unexpected difference in V_{BE} was that it was due to the base modulation (Early effect) caused by the large variation of V_{CB} . However, this difference could be explained only in part by the Early effect on the transistor. Adding the Early effect modulation to the expression of collector current of a transistor one obtains:

$$I_C = I_s \exp\left(\frac{V_{BE}}{V_T}\right) \left(1 + \frac{V_{CE}}{V_A}\right) \quad (5.1)$$

where V_A is the Early voltage [27].

From the data sheet of the 2N2222 it is found that its Early voltage is approximately 70 V, and from Eq. 5.1 it is expected that an increase of current from $IC_1 = 150\mu A$ to $IC_2 = 6.32mA$ with a simultaneous increase in V_{CE} from 0 to 25 V would result in a variation of $\Delta V_{BE} = 90.1$ mV.

Thus, from the measured data the value of V_{BE} immediately before the heat pulse, a value of $V_{BE} = 669.58$ mV would be expected if the Early effect is taken into account to model the transistor. However, the measured value $\Delta V_{BE} \approx 64$ mV is still much lower the calculated value $\Delta V_{BE} = 90.1$ mV and the difference ($90.1 - 64.0 = 26.1$) mV can only be attributed to a very fast heating of the transistor

Assuming that at the instant $t = t_0 + \delta t$ (with $\delta t \mapsto 0$) the transistor is still at the temperature T_0 , the thermal coefficient of V_{BE} can be calculated using the equation presented in Chapter 3, $dV_{BE}(T)/dT = [-V_{G0} + V_{BE}(T_0)]/T_0$, which for the measured value of $T_0 = 296$ K, results in $dV_{BE}(T)/dT = -1.77$ mV/°C.

Using this value for $dV_{BE}(T)/dT = -1.77$ mV/°C, the V_{BE} difference of 26.1 mV represents a temperature increase of 14.75°C. This calculated value is very close to the 15°C level shift that had to be applied to correct for the real transistor's temperature, indicating that the hypothesis is consistent with the measured results.

This result indicates that measuring the variation of V_{BE} during the heat pulse shall present a lower sensitivity, because this quasi-instantaneous increase in temperature will not be measured. If the measurement is taken before the heat pulse and immediately after the heat pulse, this temperature change will not be undetected and a higher sensitivity shall be obtained, although it is expected that measuring the values of V_{BE} immediately after the heat pulse can be a source of error. These conclusions can be easily inferred from the plot shown in Fig. 5.3.

The last test for the evaluation of the sensor's operation was performed with the sensor immersed in water, to observe it in an extreme situation (100% of water content in the soil). The measured result of the temperature variation is presented in Fig. 5.5.

From this curve it is possible to observe that the temperature variation measured when the transistor is inside the water is only 3.5 °C, which is much lower than the $\Delta T = 8.34^\circ C$ measured with the transistor in a completely dry soil. These preliminary results confirm that the proposed single element sensor is a low-cost, high sensitivity viable alternative to the well established dual element sensors available.

Although this measured value of the transistor inside the water has been performed just to verify the principle of operation of the sensor, a very interesting phenomena was detected during the measurement. It is known that, theoretically, testing the sensors in water could be a problem because of the heat convection that can occur, so the tests are always performed with an water-Agar solution. The water-Agar solution is a gel which has the same thermal properties of the water but does not present the heat convection problem (it is known as "immobilized water").

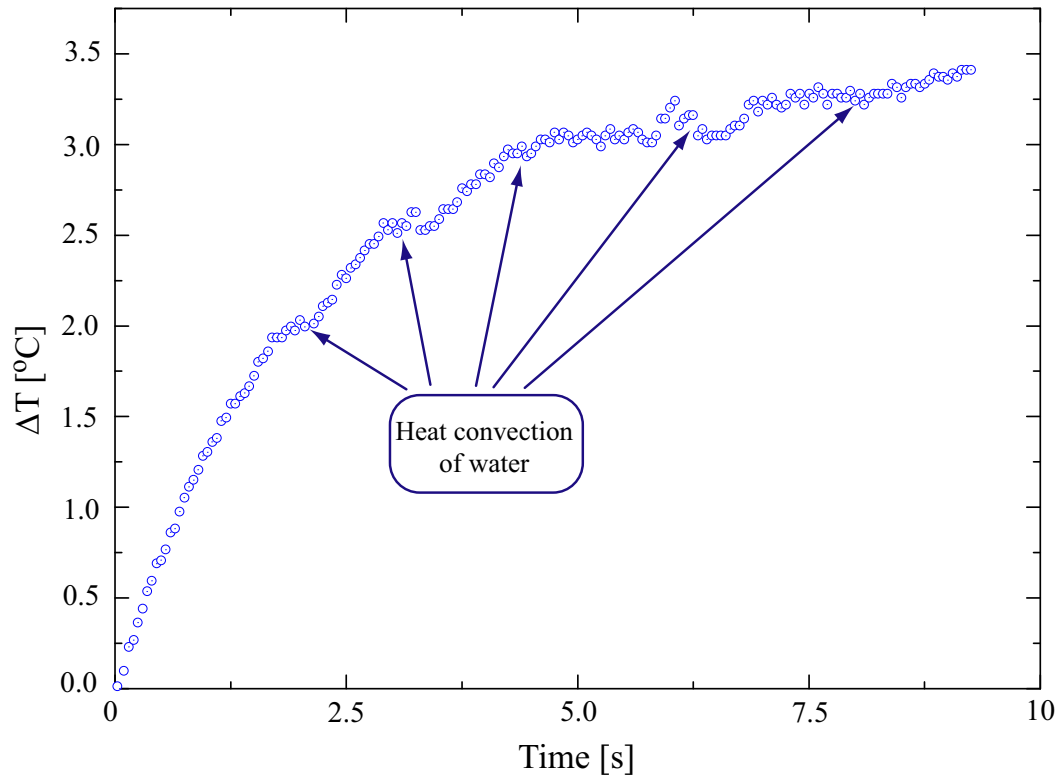


Fig. 5.5: Measured result of 2N2222 transistor immersed water.

As far we know, it is the first time that the theoretically predicted effects of fast water movement around the sensor due to the heat convection were measured. This phenomena causes an abrupt change (decrease) in the slope of the temperature curve due to the replacement of the hot water near the sensor by cold water in the bath. These changes are clearly identified in Fig. 5.5. Although the author initially imagined that the strange behavior of the curve was caused by noise or problems with the measurement set-up, the same type of curve was always present when a sensor was tested inside water. Further investigation in the literature led to conclusion that it is the heat convection in water phenomena that is being observed in these measurements.

5.2 Application of the sensor in soil moisture measurements

Soil samples prepared in ESALC [35] were used to make the tests in laboratory. The soil water retention characteristics were known, and should present $\theta_v \approx 50\%$ (when water saturated). This characteristic was confirmed by measurement in laboratory, using the following procedure.

A sample of 480 ml of soil was conditioned inside a PCV container which had a permeable material in the bottom. The soil was first oven-dried, weighted and left inside a recipient with water for 24 h, so it will be hydrated to its maximum capacity. The amount of water absorbed by the soil was 236 ml, what results in $\theta_v = 49.1\%$.

Two sensors were used to make the experimental tests in soil samples: a sensor made with a 2N2222 transistor and a sensor made with a BC547 transistor. The sensors (with the connection

wires) were inserted in small plastic cups filled with dry soil and weighted. The volume of the soil was previously measured and weighted. The weight of the plastic cup was neglected since it is less than 0.1 g.

Next the sensors were hydrated with an amount of water which would lead them to a water content just below the saturation. The samples were then weighted and left resting for 4 hours, allowing for the water to redistribute evenly inside the soil, and a first interrogation was performed.

After this, the sensors were continuously weighted (to control the amount of water) and interrogated every time a 2 g variation was observed (equivalent to 2 ml of water evaporation from the soil).

The interrogator saved and transmitted to the PC the whole set of V_{BE} data (before, during and after the heat pulse), in order to allow the study of the sensors using two techniques: temperature measurement just after the heat pulse is applied and immediately before the heat pulse is removed (as in all SPHP), and with a new technique, measuring the V_{BE} before the heat pulse is applied and after the heat pulse is removed.

This new technique theoretically presents two advantages: the first is that all measurements can be made at a low current level ($150\mu\text{A}$) and with the transistor with $V_{CB} = 0$, removing nonidealities of the transistor (Early voltage, base resistance, collector resistance and high injection effects) and leading to a accurate measurement of the V_{BE} .

The second advantage is that the “loss of sensitivity” caused by the quasi-instantaneous heating of the sensor does not happen when the measurement is made at low current levels (before and after the heat pulse is applied).

5.3 Characterization of the sensor prepared with a 2N2222 transistor

5.3.1 Measuring during the heat pulse (2N2222)

The measured result of the temperature variation of sensor labeled M7 (during the application of the 10 s heat pulse) as a function of the volumetric soil moisture content θ_v is presented in Fig. 5.6

In this figure it is possible to see that when the volumetric water content of the soil changed from $\theta_v = 0\%$ to $\theta_v = 43.8\%$, the maximum measured variation of ΔT was 4.5°C . When the agricultural range of θ_v is considered, the maximum variation observed is approximately 3.0°C (from 4.8°C to 7.8°C).

It is important to remember that 3.0°C corresponds to a variation in V_{BE} of approximately 5.7 mV and, to read these variations with 1% resolution, it is necessary to resolve $57\mu\text{V}$. As shown previously, the 16 bit A/D converter has a resolution of $18\mu\text{V}$ and the interrogator allows for low noise readings, with all readings falling inside a $54\mu\text{V}$ range, so this sensor can be used to measure the soil moisture with a 1% resolution in the agricultural range with this A/D converter.

The conventional method for determining soil moisture consists in calculating the difference in temperature ΔT between the first and the last measured points (the first measurement after the heat pulse is applied and the last measurement before the heat pulse is removed). These points (final value of ΔT) are plotted in Fig. 5.7.

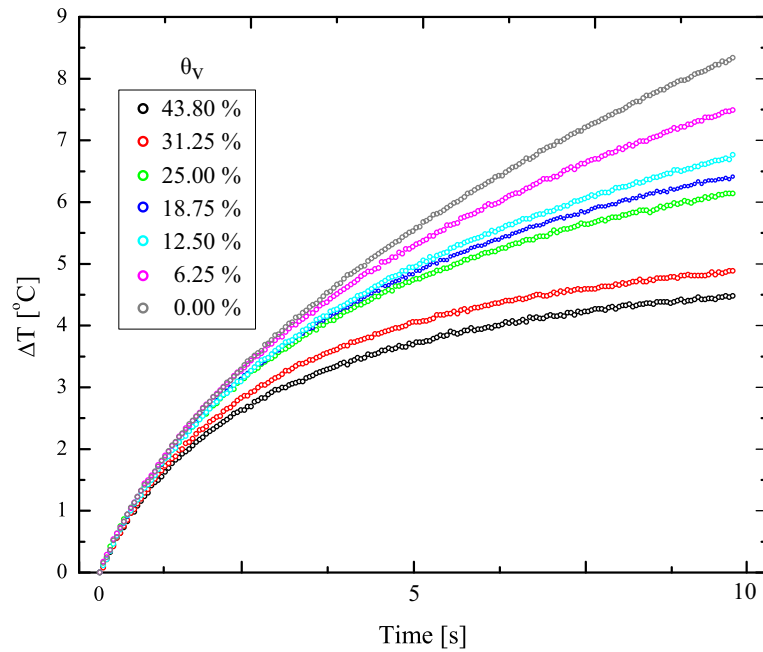


Fig. 5.6: Measured result of a sensor prepared with a 2N2222 transistor for different values of θ_v .

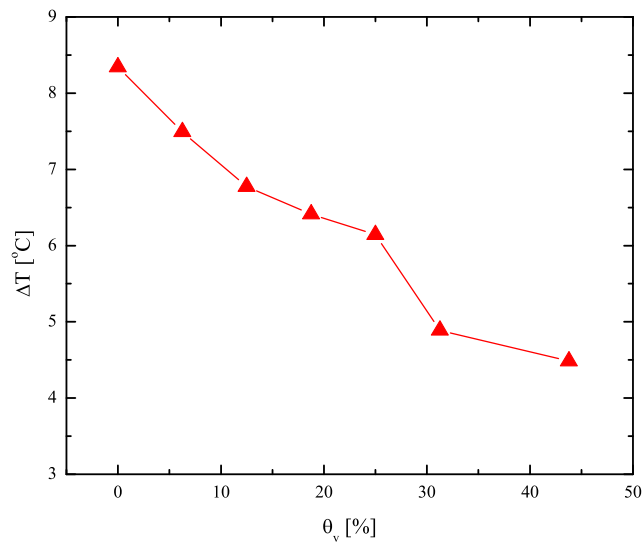


Fig. 5.7: Plot of the temperature difference ΔT as a function of soil water content θ_v for a sensor prepared with a 2N222 transistor.

It is interesting to plot the results obtained with the Campbell 229 sensor [4] and a dual probe sensor [15] to compare the curves. The comparison of the results is shown in Fig. 5.8.

The nonlinear response obtained with all sensors is evident. When compared to the 229 SPHP sensor from Campbell, it is seen that the developed sensor presents a similar behavior from θ_v between

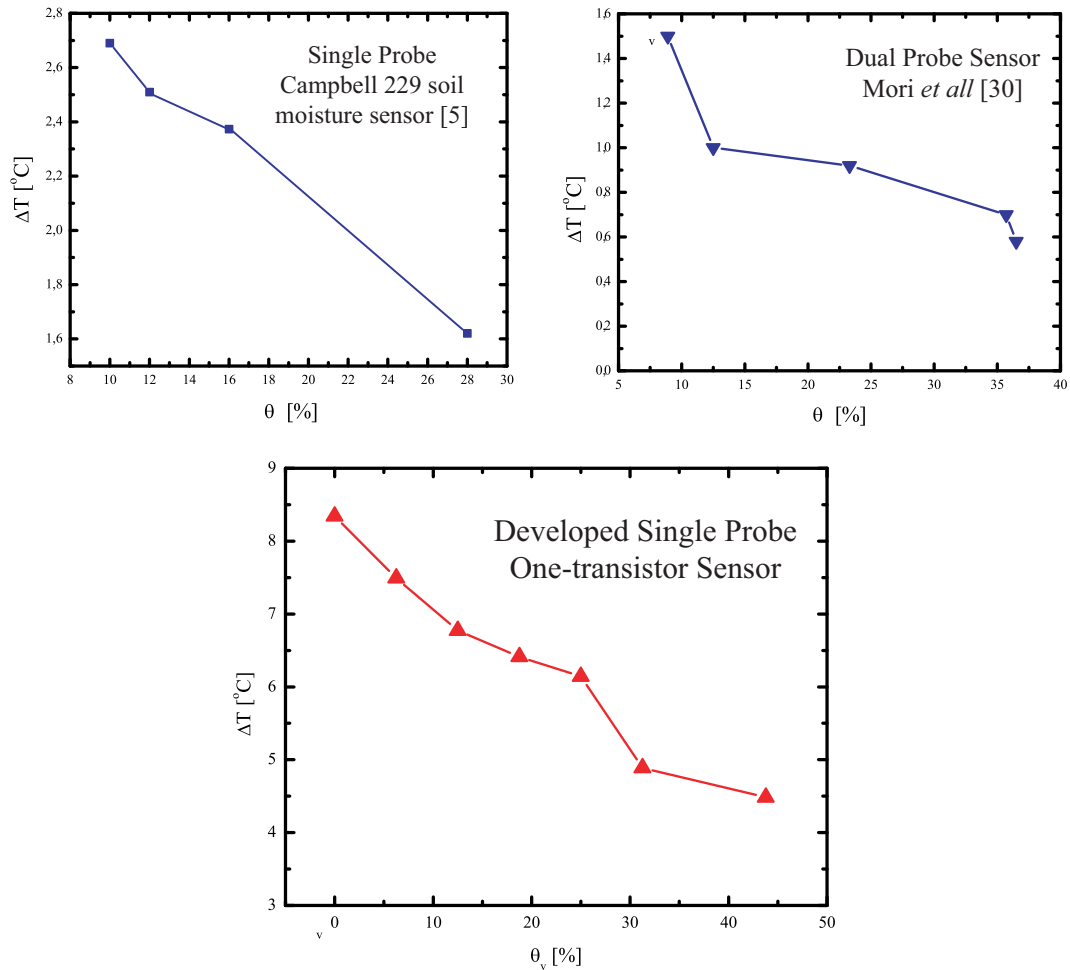


Fig. 5.8: Comparison of the measured temperature difference ΔT as a function of soil water content θ_v for three different sensors: Campbell 229 SPHP commercial sensor, a DPHP sensor presented by Mori *et al.* and the developed sensor prepared with a 2N2222 transistor.

6% and 16%, but the lack of data in the region of θ_v between 16% and 28% for the Campbell 229 does not allow for a good comparison between the curves for the rest of the range.

It is also interesting to show a plot of the resistivity of a soil, measured with another commercial sensor (Decagon KD2 Pro) [36]. The plot, presented in Fig. 5.9, shows that a very nonlinear behavior is obtained, and that this behavior depends heavily on the soil content, and that the curve of thermal conductivity *versus* θ_v may present more than one concavity. Furthermore, the mechanisms of heat transfer inside the soil depend also on the soil density [37], and the same soil compacted with different bulk densities presents a large variation of its thermal conductivity, as shown in Fig. 5.10.

Despite of the difficulty of precisely relating the values of ΔT measured (with any type of sensor) with the actual content of water in a soil, it is important to notice that using the conventional technique of measuring the temperature during the heat pulse, the developed single-element sensor in this work presents a sensitivity which is approximately 4 times better than the other sensors.

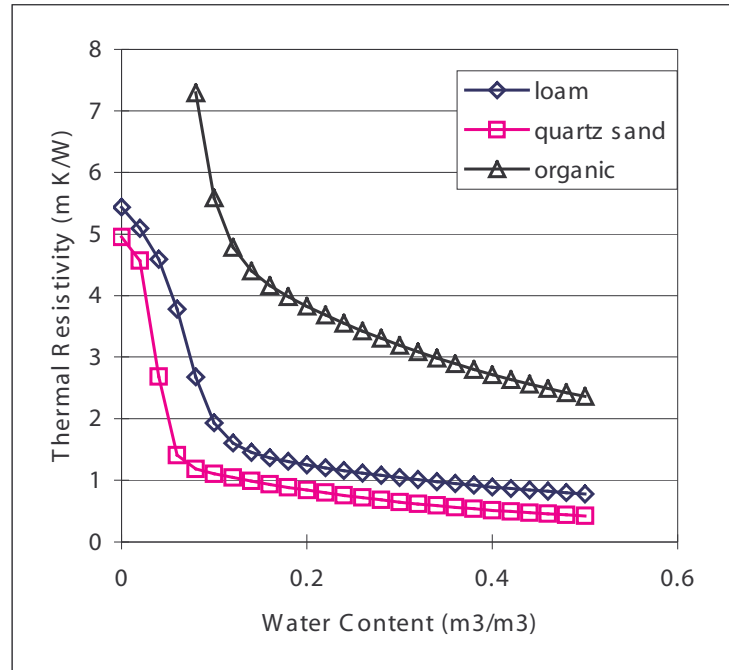


Fig. 5.9: Plot of the thermal conductivity of three types of soil: loam, quartz sand and organic

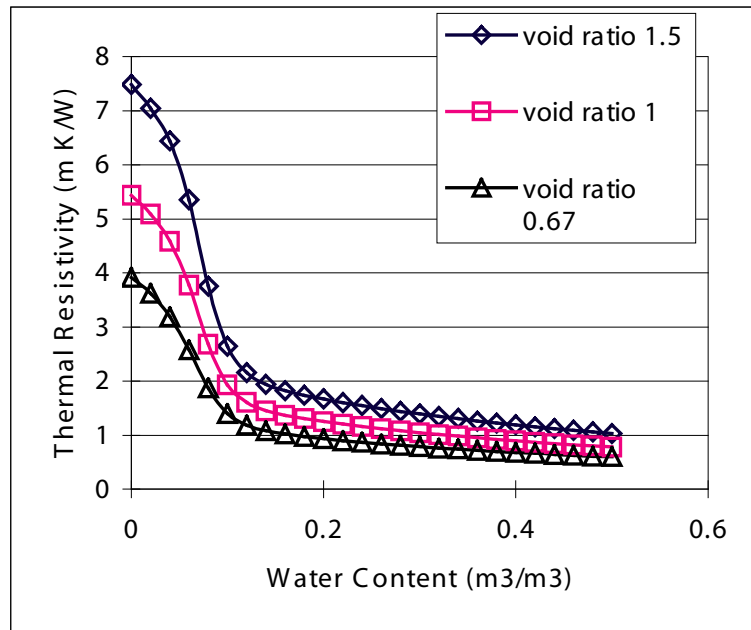


Fig. 5.10: Effect of density and water content on thermal resistivity of a loam soil. The bulk densities are 1.06 Mg/m³ for void ratio of 1.5, 1.33 Mg/m³ for void ratio 1, and 1.59 Mg/m³ for void ratio of 0.67.

5.3.2 Measuring before and after the heat pulse (2N2222)

Since it was verified that the sensor is heated up almost instantaneously, and this quasi-instantaneous heating reduces the ΔT which is possible to be measured, it is worth to try a second technique for measuring the ΔT where this fast heating will not reduce the temperature measurement range. The idea is to measure the V_{BE} before and after the heat pulse is applied, so both measurements will be performed with $V_{CB} = 0$ V and $I_C = 150\mu\text{A}$, and a larger variation of ΔT would be expected.

However, as mentioned earlier, there is a fast cool down of the sensor when the heat pulse is removed, and it is necessary to verify how this temperature change affects the measurement.

In Fig. 5.11 it is plotted the variation of ΔT after the heat pulse is removed, for various values of θ_v , as a function of the time. All curves start at $t = 18.5$ ms, since the first two measured points were discarded, since other sources of error could affect the measurement (for example, the slew-rate of the op-amp that applies the voltage pulse). As it can be noticed, the sensor cools down very quickly, and all curves have the same behavior. This indicates that that for the whole range of operation (θ_v in the range of 5% to 43.8%) it should be possible to choose any point of the measured values to calculate the soil moisture.

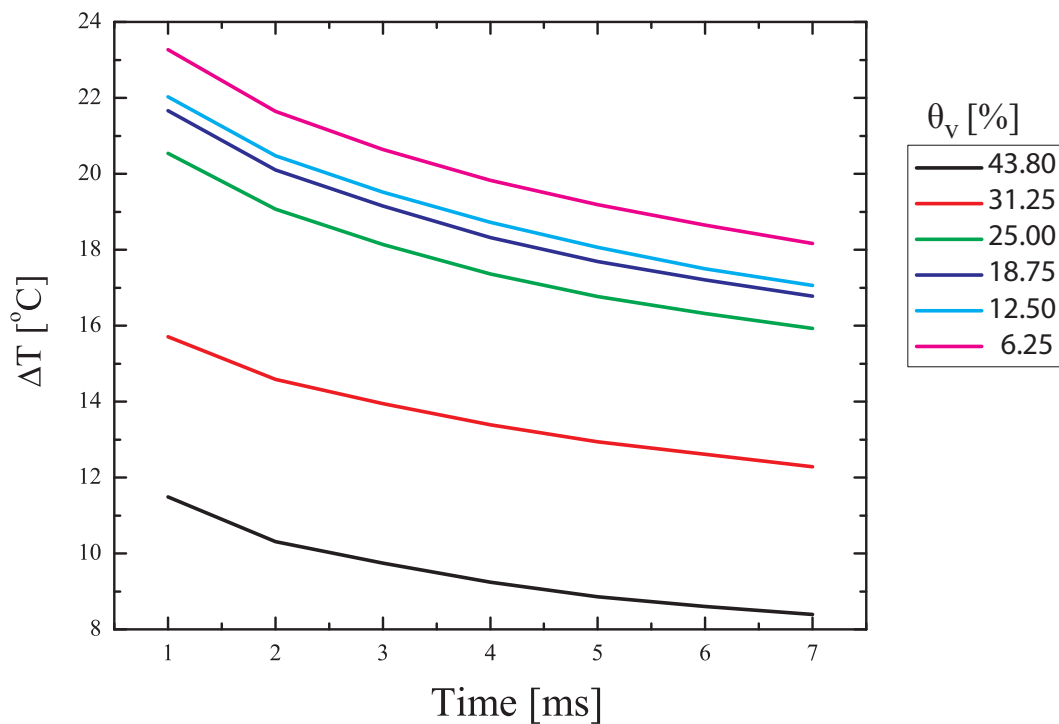


Fig. 5.11: Measured variation of ΔT (before and after the heat pulse) for various values of θ_v , as a function of the time.

The plot in Fig. 5.12, where the value of δT is a function of θ_v , for various measuring point positions is presented, confirms what a visual inspection of Fig. 5.11 indicates: discarding the first two measurements after the heat pulse is removed, the decay in temperature for the next 6 points is very similar, regardless of the water content of the soil.

A plot of the variation of ΔT as a function of θ_v in the agricultural range for the points No.3 and

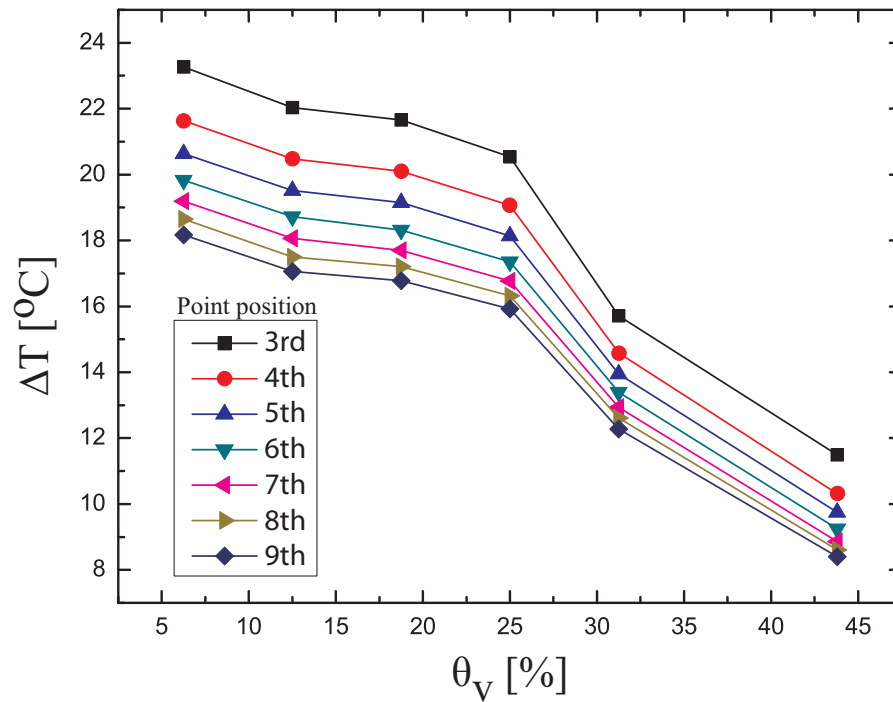


Fig. 5.12: Measured variation of ΔT (before and after the heat pulse) for each measurement point position, various values of θ_v .

point No.8 is presented in Fig. 5.13. This range of points seem to offer the best solution to: (a) avoid errors in the points acquired just after the heat pulse; (b) avoid letting the sensor to cool down too much, decreasing the temperature range of ΔT and reducing its sensitivity.

At this point it becomes clear that both curves present very similar behavior, and using the data from point No.3 will lead to a higher value of ΔT . Examining the plot of point No.3 in Fig. 5.13 it is possible to calculate a maximum value of $\Delta T = 23.2^\circ\text{C}$ for $\theta_v = 6.3\%$. Using the data acquired for point No.3, the maximum sensitivity of the sensor occurs for dry soils, and it is 79.3°C per unit change ($\text{m}^3.\text{m}^{-3}$), that is, a 1% change in the water content will result in a temperature variation $\Delta T = 0.79^\circ\text{C}$. For soils in the upper limit of the agricultural range ($\theta_v = 35\%$) the calculated sensitivity is 52.3°C per unit change ($\text{m}^3.\text{m}^{-3}$).

The sensitivity of the developed sensor is one order of magnitude higher than the best result presented in the literature for SPHP sensors, which present a sensitivity of only 7.6°C per unit change ($\text{m}^3.\text{m}^{-3}$). When compared to the DPHP sensors, the sensitivity of this new sensor is almost 20 times better, as the DPHP sensors available present a typical maximum sensitivity of 4.0°C per unit change ($\text{m}^3.\text{m}^{-3}$).

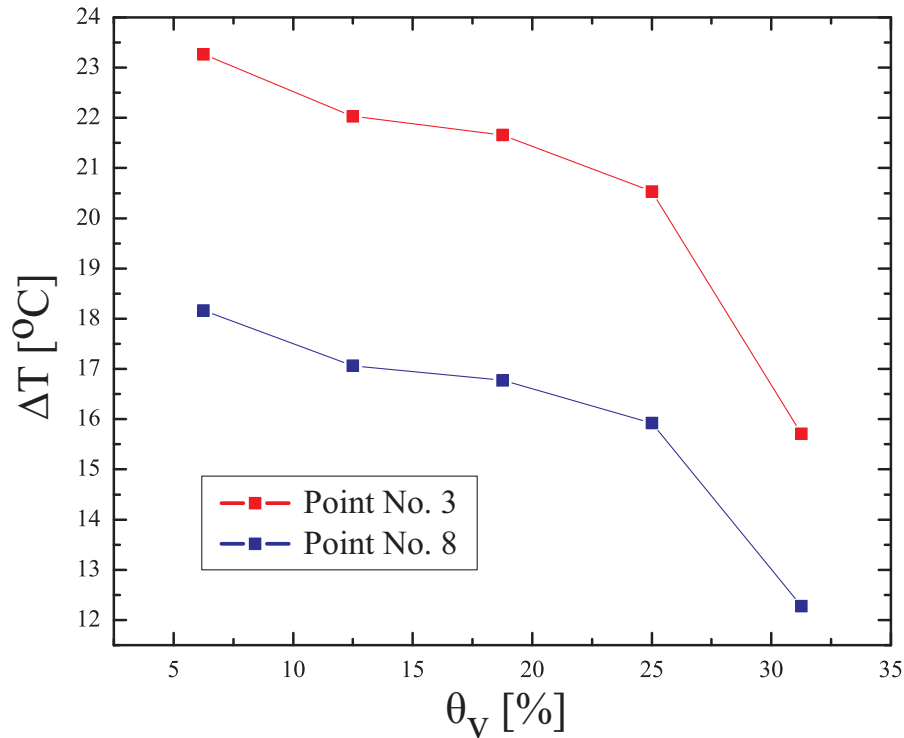


Fig. 5.13: Measured variation of ΔT (before and after the heat pulse) for point No. 3 and point No. 8, for various values of θ_V .

5.4 Characterization of the sensor prepared with a BC547 transistor

In order to study the influence of the packaging of the transistor in the sensor's performance, BC547 transistors, which have a plastic package, were also tested, and the same measurements were performed.

It is possible to predict that the response of this plastic transistor will be significantly different from the metal can 2N2222 transistor, since the data-sheets of these devices show that the thermal resistance of both packages are very different: the thermal resistance (junction to ambient) of the BC547 is $R_{THja} = 250^\circ\text{C/W}$ and the the 2N2222 has $R_{THja} = 383^\circ\text{C/W}$.

A lower thermal resistance indicates that the heat transfer to the soil will be more efficient, and lower values of ΔT are expected in sensors prepared with the BC547 transistors. The variation in the thermal capacity (the BC 547 has a large mass of epoxy acting as a heatsink) shall also change the time constant of the sensor.

5.4.1 Measuring during the heat pulse (BC547)

The first measurement was made just to verify the functionality of the sensor. The results of a test with the sensor in the air and inserted in a dried soil is presented in Fig. 5.14. It is noticed that the sensor works correctly and, as expected due to its lower thermal resistance, the maximum temperature

reached after 10 s of heat pulse (9.8 °C in the air and 6.1 °C in the dry soil) are respectively 0.4 °C and 2.2 °C lower than the ΔT found in the 2N2222 transistor.

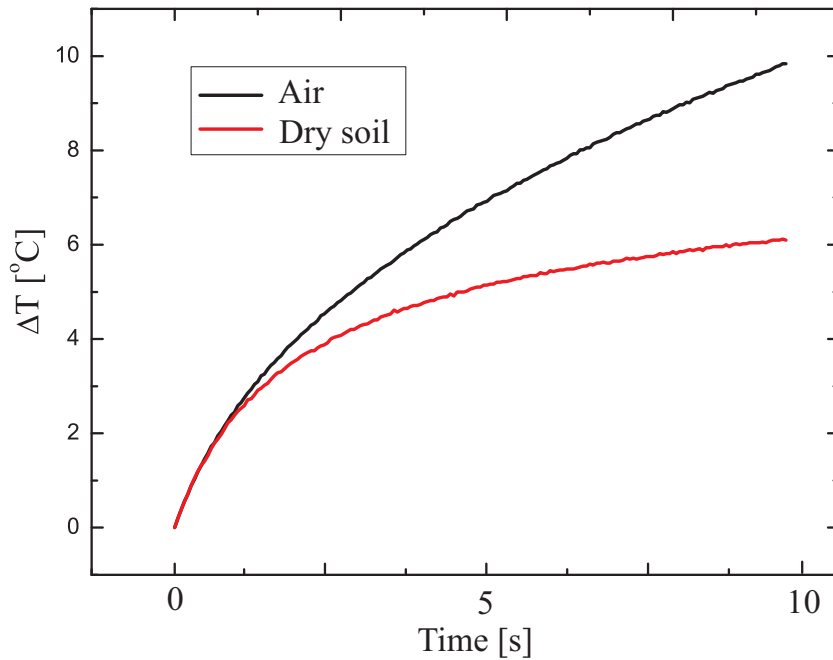


Fig. 5.14: Measured variation of ΔT in the sensor prepared with a BC547 transistor in the air and into a dry soil.

A measurement with the transistor immersed into the water was also performed, to verify if the phenomena of water convection also occurs with this plastic package. The measured results are presented in Fig. 5.15, where it is observed that the water convection is still possible to be noticed.

The sensor prepared with the plastic package transistor was tested in the whole agricultural range, using the same experimental procedure employed in the measurement of the sensor with the metallic 2N2222 transistor, and the results are presented in Fig. 5.16.

Observing the results, it is seen that the maximum value of ΔT was 5.0 °C (which is much lower than the $\Delta T = 7.5^\circ\text{C}$ found with the 2N2222 sensor), confirming the theoretically predicted lower sensitivity, due to the lower thermal resistance. Besides this loss in sensitivity, a problem is found when measuring a soil with high water content ($\theta_v = 37.5\%$), since it can be observed in the presented curve that the phenomena of water movement in the soil is present, a known source of errors in determining soil moisture.

A plot of ΔT (last point measured immediately before the heat pulse is removed) as a function of θ_v is presented in Fig. 5.17.

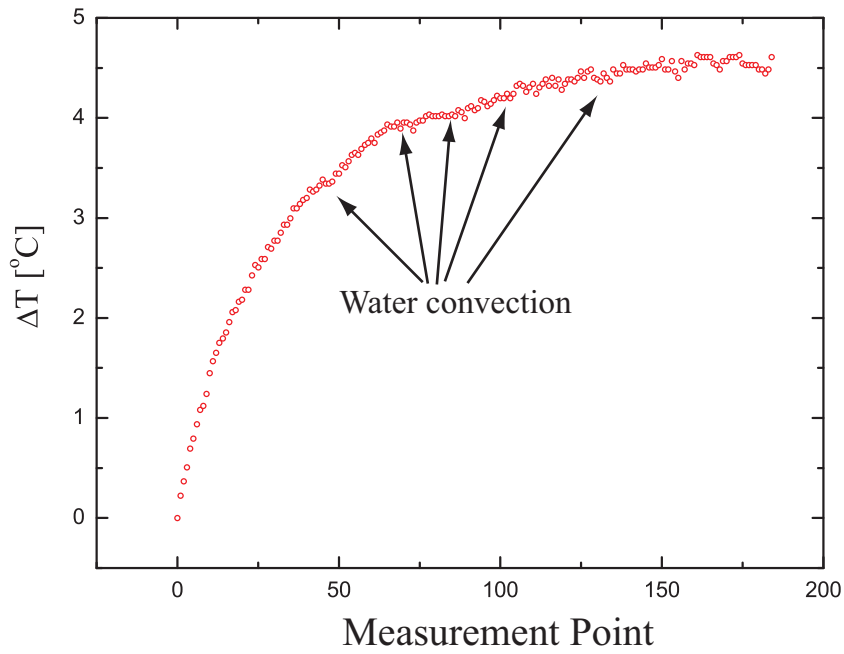


Fig. 5.15: Measured variation of ΔT in the sensor prepared with a BC547 transistor immersed in water.

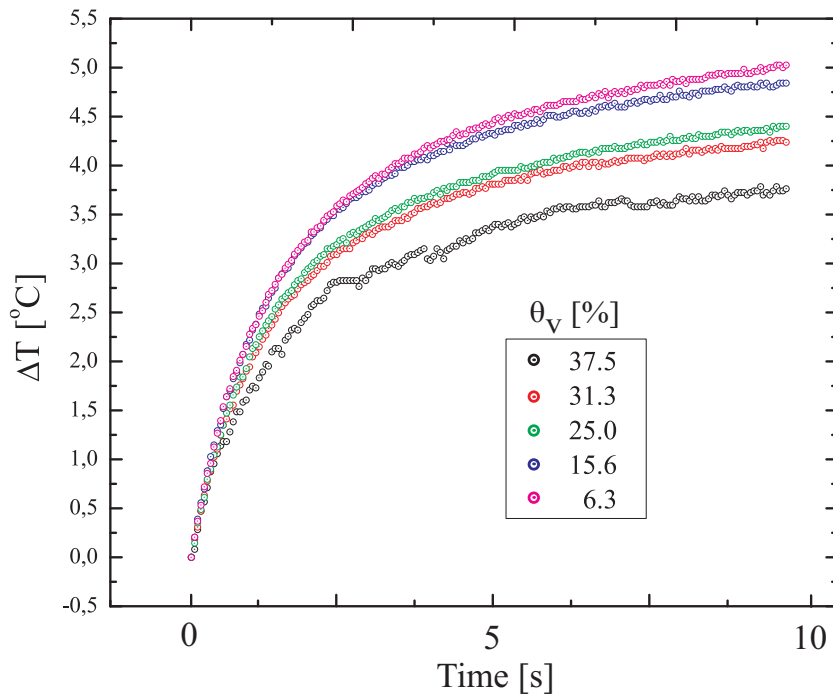


Fig. 5.16: Measured variation of ΔT as a function of the time, for the sensor prepared with a BC547 with various θ_v .

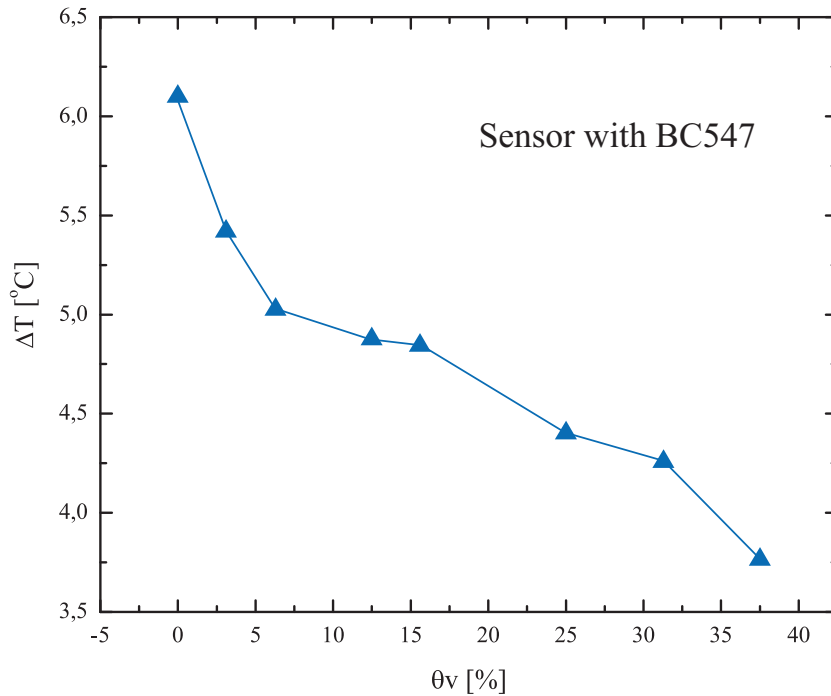


Fig. 5.17: Measured variation of ΔT in the sensor prepared with a BC547 transistor as a function of θ_v .

5.4.2 Measuring before and after the heat pulse (BC547)

In Fig. 5.18 it is plotted the variation of ΔT , for various values of θ_v , as a function of the time. The measurement protocol was exactly the same used with the 2N222 transistor. All curves start at $t = 1.14$ ms and the first two measured points were discarded. Here it becomes evident that the different thermal properties of the plastic package have a large influence in the sensor's behavior.

Examining the curves in Fig. 5.18 it can be noticed that the thermal capacity of the plastic package introduces a delay in the thermal behavior of the sensor and, depending on the soil moisture, the slope of the curve is positive or negative for this small period of time analyzed.

For values of θ_v above 25 % the temperature of the sensor decreases after the heat pulse is removed, whilst for θ_v below 25 % the temperature of the sensor continues to increase. Of course this increase in temperature occurs only for a very small period of time, but this phenomena can lead to inaccuracies in the measurement. Of course that delaying the measurement to avoid picking up a point while the sensor is still heating up would be a solution, however, as shown earlier, this would decrease the sensor's sensitivity.

The plot of the points No.3 and points No.8 is presented in Fig. 5.19. The crossing of the curves occurs because of the slope change of the curves.

It was shown that the SPHP sensor prepared with a plastic package transistor presents a lower sensitivity (the metallic package presented a maximum sensitivity which is 50% higher) and also that the thermal properties of the package introduces thermal delays that results in inaccuracies in the association of ΔT with water content in the soil θ_v .

From these findings, it seems that there is not any advantage in using the plastic package transis-

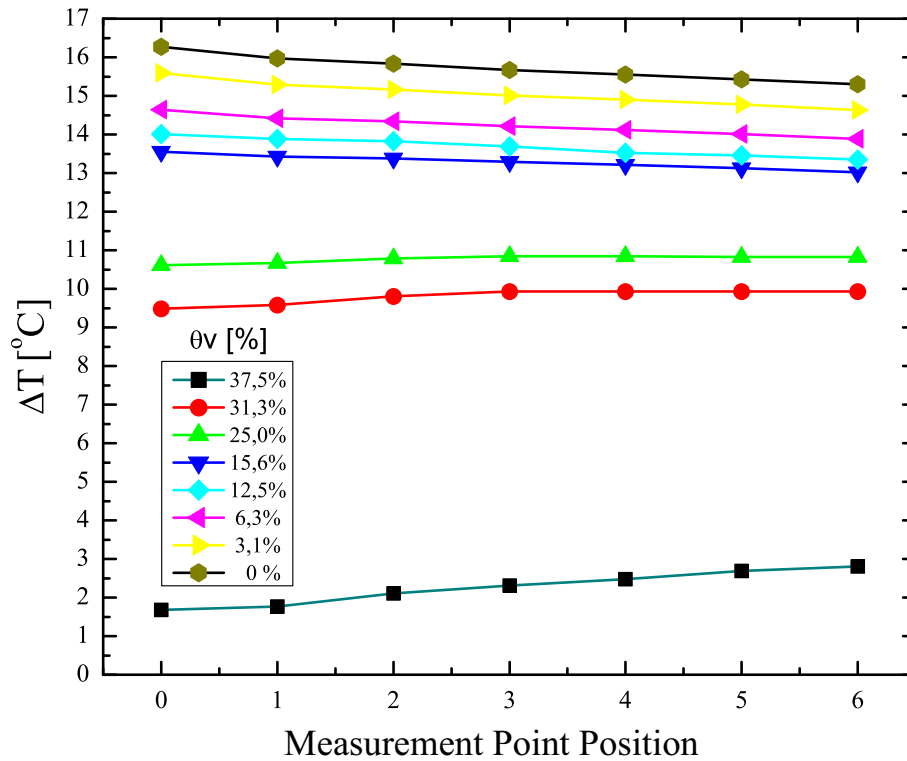


Fig. 5.18: Measured variation of ΔT (before and after the heat pulse) for each measurement point position, various values of θ_v (BC547).

tors to make the SPHP soil moisture sensors, and further investigations must be conducted if for any reason it is desired to use transistors with plastic packages.

Finally, the sensors which were encased in a porous gypsum block were also tested. Both plastic (BC547) and metallic (2N2222) transistors were used to prepared the gypsum block sensors. In Fig. 5.20 it is plotted the variation of ΔT for three values of θ_v (dry, intermediate and saturated) for the gypsum block with a 2N2222 transistor. In Fig. 5.21 it is plotted the same curve for the gypsum block with a BC547 transistor.

The measurement of the sensor prepared with a gypsum block showed problems with both transistors. Although both sensors worked well for low water contents, both presented problems when saturated with water.

The sensor with the plastic package transistor (BC547) when saturated with water showed a curve that is impossible to be used to make any reading of temperature. The sensor with the metallic package transistor (2N2222) when saturated with water showed a curve that presents a clear instability near the end of the heat pulse. The pattern of heating and cooling of the junction of the transistor found in the measurements with the sensors saturated, indicates that there is water movement inside the gypsum porous block.

This characteristic was observed in many sensors, and further investigation must be conducted to fabricate sensors with the proposed technique using gypsum porous blocks. A decrease in the power applied to the transistor was a solution that effectively worked and reduced/eliminated the water's movement inside the porous block, but this solution brings an associated loss of sensitivity. Another

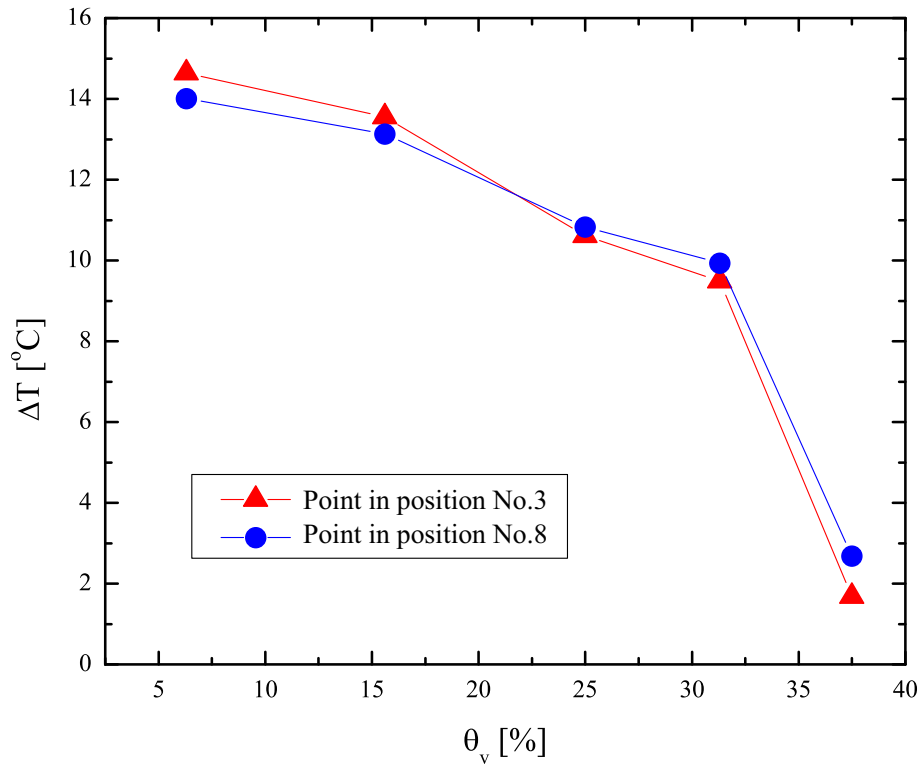


Fig. 5.19: Measured variation of ΔT (before and after the heat pulse) for measured points in position No.3 and No.8, as a function of θ_v (BC547).

possible solution would be changing the porosity of the gypsum block, but this is far beyond the scope of this work.

Since soil moisture sensors prepared with gypsum blocks present many weaknesses (they deteriorate with time, the porosity changes with time because the porous become obstructed by soil particles, they are much larger and weight more than the single transistor sensors), it seems that future applications of this developed technique will be focused on the use of single transistors, without any porous material around them.

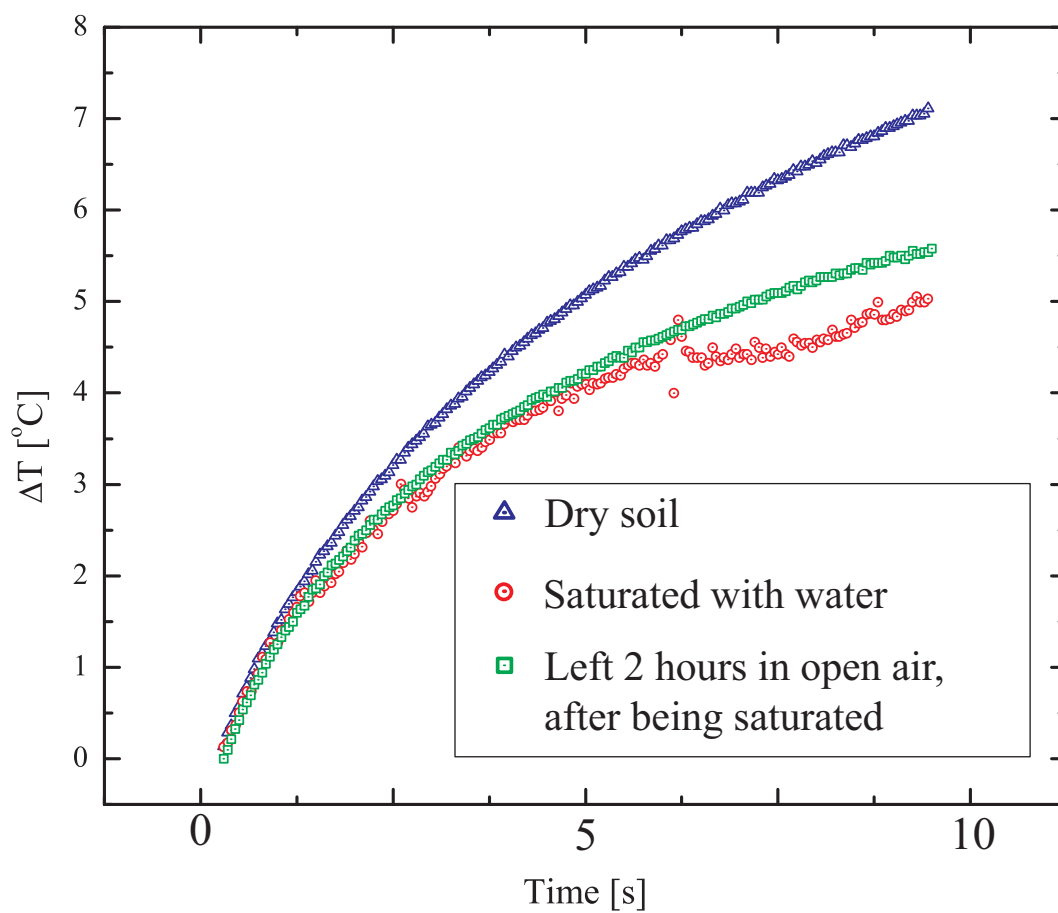


Fig. 5.20: Measured variation of ΔT (during the heat pulse) for three values of θ_v , as a function of the time (2N2222).

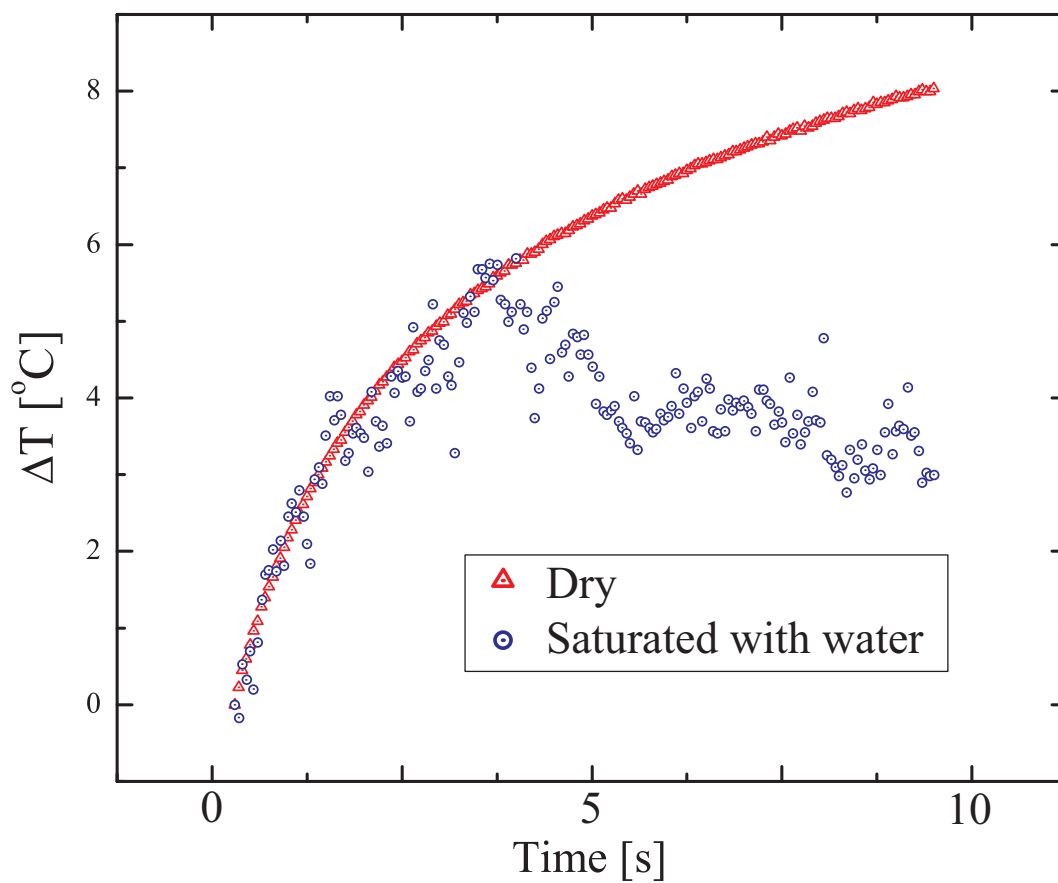


Fig. 5.21: Measured variation of ΔT (during the heat pulse) for three values of θ_v , as a function of the time (BC547).

Chapter 6

Conclusions

THE classic technique for measuring soil water content using heat transfer properties was employed to develop a new single probe heat pulse sensor. The novel sensor is comprised of only one element, a *npn* junction bipolar transistor, which works as both heating and temperature sensing elements. The variations of V_{BE} as a function of the temperature are used to measure the temperature of the sensor and, since the behavior of $V_{BE}(T)$ is one of the most well studied expressions that describe the bipolar transistor, the sensor's temperature can be measured with high accuracy.

The fabrication of bipolar transistors is well dominated since the end of the 1960s. Because of the fact that fully automated manufacturing techniques are used to package the transistors, the mechanical and thermal behavior of all transistors manufactured by a same silicon foundry are virtually identical, resulting in sensors with the same thermal behavior. Modern technologies produce transistors with electrical characteristics extremely well matched, and sensors manufactured using these well controlled transistors would not require any type of calibration.

An ingenious technique of increasing simultaneously the voltage V_{CB} and the collector current I_C of the transistor allows for the application of the heat pulse with low level currents, in the order of 6 mA, while the conventional heat pulse sensors use currents in the range of 50 mA to generate the heat pulse. This results in a long battery life for the interrogator circuit. A dc-dc converter was used to generate the 25 V voltage required to apply the heat pulse.

The sensor developed is very small, lightweight, low-cost, and requires only 6 mA to create the heat pulse. Therefore, it is adequate not only to be used in the crop fields, but also in space flight applications, where the culture of plants in microgravity is being investigated, for future long-term self-sustainable space missions. Although not too much information has been revealed from the TMAS sensor [17] currently under test by NASA, since it uses a NiCr resistor encased together with a thermistor, it is expected that the thermal behavior will not be very different from the conventional SPHP or DPHP, and a current in the order of several tens of mA must be used to heat the sensor.

The sensor developed in this work presented a sensitivity of 79.3°C per unit change ($\text{m}^3.\text{m}^{-3}$) for soils in the lower limit of the agricultural range ($\theta_v = 5\%$) and, for soils in the upper limit of the agricultural range ($\theta_v = 35\%$), the calculated sensitivity is 52.3°C per unit change ($\text{m}^3.\text{m}^{-3}$).

These figures are one order of magnitude higher than the best result presented in the literature for SPHP sensors, which present a sensitivity of only 7.6°C per unit change ($\text{m}^3.\text{m}^{-3}$) for $\theta_v = 5\%$. When compared to the DPHP sensors, the sensitivity of this new sensor is almost 20 times better, as the DPHP sensors available present a typical maximum sensitivity of 4.8°C per unit change ($\text{m}^3.\text{m}^{-3}$).

for the same $\theta_v = 5\%$.

When compared to the dual/multiprobe heat pulse sensors, they are much easier to be fabricated (the only procedure is to solder the terminal wires and apply a film of insulator to these connections, for example a silicone), do not require calibration and do not present measurement errors due to the deformation of the probes experienced by the SPHP or MPHP sensors when inserted into a soil.

A simple electro-thermal model was developed and experimental results show that the model can be used to predict the thermal behavior of a sensor using circuit SPICE-like simulators. Two types of sensors were prepared, using a metal can package transistor and a plastic package transistor. The developed electric-thermal model showed that the plastic package transistor should present a lower sensitivity, and this was verified experimentally. The sensors that used the plastic transistors presented a poor behavior when measuring soils with high water content, since they produced the convection of water which was near the surface of the sensor.

A couple of sensors were also prepared using a gypsum porous block, just to investigate the behavior of this new technique in conventional porous block sensors. The tests were performed motivated mostly by scientific curiosity, because the porous blocks made of ceramic or gypsum have a short life in the field (they deteriorate with time and get obstructed by soil particles, changing its thermal characteristics) and, due to its size and weight, are not adequate for space flight applications.

The results obtained with the gypsum porous block showed that the sensors worked, but the movement of water inside the porous block when the sensors are saturated with water can jeopardize the result of the measurement. A different technology for the fabrication of the porous block (controlling the size of the porous) or a decrease in the heat pulse would be necessary to make these porous block sensors operate correctly.

An interrogation technique was developed and an electronic circuit was designed, implemented and tested. The circuit is powered by batteries and, due to the low current interrogation technique developed, the battery durability is expected to be months before a recharge is required. The circuit uses a MSP430FE251 microcontroller to manage the measuring operations and to make the A/D conversion (with 16 bits) for reading the V_{BE} values.

An USB-UART converter (FT232RL) was used to transmit the data stored in the microcontroller to a PC computer, using the USB port. An especial strategy was used in the management of the measurement, and the USB port and the dc-dc converter were turned-off during the whole phase of measurement, resulting in a very low-noise system. The A/D conversions of a stable voltage showed that the measurement fluctuation fell within a 3 LSB band (all measurements fell inside a $54.9\mu\text{V}$ band).

A LabView program was developed to read and process the V_{BE} data sent by the interrogator, calculating the temperature of the sensor and showing the maximum value of ΔT . Using the LabView to automatically read and process the data during the laboratory experiments for the characterization of the sensors was fundamental, since hundreds of measurements were made in many different sensors.

Finally, it is important to observe that this work has presented only the basis for the development of SPHP sensors using a single transistor as the heating and sensing element, and much further investigations must be carried out to optimize the sensor.

The technique continues to be investigated, in a Ph.D. work in the Department of Electronics and Microelectronics DEMIC/FEEC. In this Ph.D. work the influence of parameters like time of heating, heating power, initial stand-by current, measurement point position, initial heating phenomena are being studied, using the electronic interrogator developed and the preliminary knowledge acquired

with this work.

Another possible utilization for this work is the development of a thermal property analyzer, an equipment which is used not only in the agricultural field but also by engineers that need a portable field or laboratory device to measure thermal conductivity, resistivity, diffusivity, and heat capacity. Since many of these equipments use the SPHP technique together with a microprocessor to calculate the thermal parameters of the material being tested, the developed sensor has all the features required to implement a thermal property analyzer.

Bibliography

- [1] D. Nielsen, J. Biggar, and K. Erh, "Spatial variability of field-measured soil-water properties." *Hilgardia*, vol. 42(7), pp. 215–259, 1973.
- [2] Wilson and Scott, "Concepts of variable rate technology with considerations for fertilizer application," *Journal of Production Agriculture*, vol. 7, no. 2, pp. 195–201, 1982.
- [3] *Evaluation of Phosphorus Management and Critical Soil Test Levels for Corn In the Northern Corn Belt.*, Cincinnati, Ohio, 2012.
- [4] C. Scientific, *229 Heat Dissipation Matric Water Potential Sensor Instruction Manual*, 2006.
- [5] S. L. D.L. Corwin, "Characterizing soil spatial variability with apparent soil electrical conductivity." *Computers and Electronics in Agriculture*, vol. 46), pp. 103–133, 2005.
- [6] J. M. Hubbell and J. Sisson, "Advanced tensiometer for shallow or deep soil water potential measurements," *Soil Science*, vol. 163, no. 4, pp. 271–277, April 1998.
- [7] E. Greacen, "Soil water assessment by the neutron method," *CSIRO Melbourne*, 1981.
- [8] D. Robinson, T. Kelleners, J. Cooper, C. Gardner, P. Wilson, I. Lebron, and S. Logsdon, "Evaluation of a capacitance probe frequency response model accounting for bulk electrical conductivity: Comparison with tdr and network analyzer measurements," *Vadose Zone Journal*, pp. 992–1003, November 2005.
- [9] M. Seyfried, "Field calibration and monitoring of soil-water content with fiberglass electrical resistance sensors," *Soil Sci. Soc. Am. J.*, vol. 57, pp. 1432–1436, 1993.
- [10] J. W. G.S. Campbell, C. Calissendorff, "Probe for measuring soil specific heat using a heat-pulse method," *Soil Sci. Soc. Am. J.*, vol. 55, pp. 291–293, 1991.
- [11] D. D. Vries, *Thermal properties of soil*, ser. W.R. van Wijk. New York: John Wiley and Sons, 1963, pp. 210–234.
- [12] Y. Song and G. K. J.M. Ham, M.B. Kirkham, "Measuring soil water content under turfgrass using the dual-probe heat-pulse technique," *J.Amer.Soc.Hort.Sci.*, vol. 123, pp. 937–941, 1998.
- [13] J. M. H. Julie M. Tarara, "Measuring soil water content in the laboratory and field with dual-probe heat-capacity sensors," *Agronomy Journal*, vol. 89, pp. 535–542, 1997.

- [14] A. Valente, R. Morais, C. Couto, and J. H. Correia, "Modeling, simulation and testing of a silicon soil moisture sensor based on the dual-probe heat-pulse method," *Sensors and Actuators A*, vol. 115, pp. 434–439, 2004.
- [15] Y. Mori, J. W. Hopmans, A. P. Mortensen, and G. J. Kluitenberg, "Multi-functional heat pulse probe for the simultaneous measurement of soil water content, solute concentration, and heat transport parameters," *Vadose Zone Journal*, vol. 2, pp. 561–571, 2003.
- [16] J. A. S. Dias, W. Roque, F. W. D. Pfrimer, and E. C. Ferreira, "A combined wenner-array/heat dissipation sensor for measuring electric conductivity and moisture of soils." in *Proceedings of the CIGR*, vol. 125, 2009.
- [17] M. A. Ask, J. J. Prenger, D. Rouzan-Wheeldon, V. Rygalov, J. Norikane, and H. Levine, "Investigating local impacts of heat-pulse sensors for media moisture content," *Gravitational and Space Biology*, 2006.
- [18] J. H. Norikane, J. J. Prenger, D. T. Rouzan-Wheeldon, and H. G. Levine, "A comparison of soil moisture sensors for space flight applications," *Applied Engineering in Agriculture*, vol. 21, pp. 211–216, 2005.
- [19] J. Ham and E. Benson, "On the construction and calibration of dual-probe heat capacity sensors," *Soil Science Society of America Journal*, vol. 68, pp. 1185–1190, July-August 2004.
- [20] P. C. Dias, W. Roque, E. C. Ferreira, and J. A. S. Dias, "Proposal of a novel heat dissipation soil moisture sensor," in *Proceedings of the 5th International Conference on Circuits, Systems and Signals (CSS'11)*, September 2011, pp. 124–127.
- [21] C. J. Phene, G. J. Hoffman, and S. Rawlins, "Measuring soil matric potential in situ by sensing heat dissipation within a porous body," *Soil Sci. Soc. Am Proc.*, vol. 35, pp. 27–33, 1971.
- [22] A. Valente, R. Morais, C. Couto, and J. H. Correia, "Modeling and simulation of a silicon soil moisture sensor based on the dphp method for agriculture," *EUROPEAN CONFERENCE ON SOLID-STATE TRANSDUCERS*, vol. 17, pp. 564–567, 2003.
- [23] L. Technologies, "Ltspace iv," January 2012. [Online]. Available: <http://www.linear.com/designtools/software/#LTspace>
- [24] P.-Y. Sulima, H. Beckrich, J. L. Battaglia, and T. Zimmer, "Self-heating investigation of bulk and soi transistors," *AK-MOS*, April 2005.
- [25] J. W. Hopmans, J. Šimunek, and K. L. Bristow, "Indirect estimation of soil thermal properties and water flux using heat pulse probe measurements: Geometry and dispersion effects," *Water Resources Research*, vol. 38, January 2002.
- [26] M. Gunawan, G. C. M. Meijer, J. Fonderie, and J. H. Huijsing, "A curvature-corrected low-voltage bandgap reference," *IEEE JOURNAL OF SOLID-STATE CIRCUITS*, vol. 28, no. 6, pp. 667 – 670, JUNE 1993.

- [27] B. J. P., “Contribution à l’étude physique des transistors bipolaires,” Ph.D. dissertation, Université Paul Sabatier de Toulouse, 1977.
- [28] M. A. Perkins and J. H. Huijsing, *Precision temperature sensors in CMOS technology*. Springer, The Netherlands, 2066.
- [29] L. Technology, *LTC 1144*, 2012. [Online]. Available: <http://cds.linear.com/docs/Datasheet/lt1144.pdf>
- [30] F. S. Datasheet, *MBR735 - MBR760 Schottky Rectifiers*.
- [31] L. T. Datasheet, *LT3008 Series 3uA IQ, 20mA, 45V Low Dropout Linear Regulators*, 2007.
- [32] A. Devices, *ADG819/ADG820 0.5 Ohm CMOS 1.8 V to 5.5 V 2:1 Mux/SPDT Switches Data-Sheet*, 2002.
- [33] L. Technology, *LT1004 Micropower Voltage Reference*, 1985.
- [34] FTDI, “Ft232bm usb uart (usb - serial) i.c.” Future Technology Devices International Ltd., Tech. Rep., 2005, <http://www.ftdichip.com/>.
- [35] A. Durigon I and Q. de Jong van Lier II, “Determinação das propriedades hidráulicas do solo utilizando tensiômetros de polímeros em experimentos de evaporação,” *Revista brasileira de ciêncai do solo*, vol. 35, no. 4, 2011.
- [36] D. D. Inc., *Decagon KD2 Pro Thermal Properties Analyzer Operator’s Manual*, 2011.
- [37] G. Campbell, “Thermal resistivity of porous materials (soils) change with changes in density, water content, temperature and composition.” 2006.